UNIVERSITY OF MINNESOTA
ST. ANTHONY FALLS HYDRAULIC LABORATORY

Project Report No. 320

EXPERIMENTAL AND THEORETICAL STUDIES OF BANK EROSION IN RIVERS AND ITS PREVENTION BY LOW-COST MEANS

by

Norihiro Izumi, Agnes Kovacs,

Gary Parker, and David P. Leuthe

Prepared for

Legislative Commission on Minnesota Resources
State of Minnesota
St. Paul, Minnesota
[M.L. 89, Chapter 335, Sec. 29, Subd. 11I]

July, 1991

Minneapolis, Minnesota

ABSTRACT

The present report is devoted to the topic of river bank erosion and its prevention. Emphasis is placed on a physically–based model of bank erosion, into which various kinds of bank protection can be imbedded. For simplicity, the study is restricted to straight channels. The methods developed here can, however, be applied to the broader context of meandering channels.

The report consists of two parts. The first part is devoted to an experimental study of the problem. The process of bank erosion of coarse material is first studied. The channel is allowed to erode until such point as a stable equilibrium is attained. Such experiments provide a baseline against which to test the effectiveness of various means of bank protection. The type of bank protection studied falls under the category of distributed drag. Such methods use timber–pile permeable dikes, jacks, jetties, or trees in conjunction with the Palmiter method to slow the flow down in the vicinity of the bank. In the present study, screens similar to permeable dikes were used to accomplish this. It was shown that a sufficient density of distributed drag elements can substantially slow or stop bank erosion. When fine, suspendable material was added to the water, this material tended to settle out preferentially in the near–bank field of retarded velocity due to distributed drag. As a result, not only could bank erosion be prevented, but eroded banks could be reconstructed by means of deposition from suspension.

The second part of the study was devoted to a theoretical and numerical model of bank erosion and its prevention, in parallel with the experiments. The theory is based on a description of bedload transport on side slopes up to the angle of repose. The Finite Element Method was used to model the flow and sediment transport field, as well as describe the time evolution of the channel. At present, the model has proved successful in describing the process of bank erosion documented in the experiments. Numerical work continues on the subject of bank protection by means of distributed drag.

ACKNOWLEDGMENTS

Laboratory experiments were supported by grants from the Legislative Commission on Minnesota Resources, State of Minnesota [M.L. 89, Chapter 335, Sec. 29, Subd. lll]. The computation of the numerical modeling was carried out on the GRAY X–MP of the University of Minnesota, Minnesota Supercomputer Institute.

The experiments reported here would not have been possible without the help of Aaron Buesing and Amy Hansen. Their efforts are greatly appreciated. Preliminary design work for the experiments was also performed by Agnes Kovacs. Pat Swanson edited the text of this report.

TABLE OF CONTENTS

LIST OF FIGURES

List of Tables

PART 1

EXPERIMENTAL STUDY OF BANK EROSION AND ITS PREVENTION WITH DISTRIBUTED DRAG METHODS

1.1 INTRODUCTION

Alluvial rivers are dynamic in nature, constantly changing their bed and bank configurations by means of erosion and deposition of sediment. The result is a tendency toward channel shift. This shift is an inevitable and natural process that is vital to the renewal and maintenance of floodplain habitat. On the other hand, the bank erosion concomitant with river channel shift can also endanger such man–made floodplain structures as bridges, roads, and water intakes, as well as destroy arable land.

The most common river type in Minnesota is the meandering sand–bed stream. Recently MacDonald, Parker and Leuthe (1991) have completed a survey of channel shift on sixteen streams of this type in Minnesota. Rates of channel shift were found to range from 0.1 to 2 meters per year. While these values may appear to be small on an annual basis, they extrapolate to yield significant amounts of bank erosion over a thirty or forty–year period. Few floodplain structures are designed to last a shorter time than this.

A fairly classical example of problems in Minnesota caused by channel shift is provided by Parker (1982). As of 1980, the west approach to the bridge on State Highway No. 93 crossing the Minnesota River at Le Sueur was severely endangered by channel shift. This process is documented in Figure 1.1.

A study of the problem indicated that the installation of a series of short rock spur dikes near the bridge, as shown in Figure 1.2, could likely alleviate the problem. A series of four such rock spur dikes were installed in 1983 (Figure 1.3). They have served to halt bank erosion and protect the western approach to the bridge.

Rock spur dikes constitute an example of a fairly low–cost technique that can be used to protect river banks against erosion. A compendium of other low–cost techniques can be found in Bentley, Parker, and Leuthe (1991).

The development and application of low–cost bank protection techniques is particularly important in Minnesota because of the large number of actively migrating streams and the relatively low population density. High–cost techniques such as extensive bank riprapping are generally cost–effective only in urban areas, and even there can serve to seriously degrade the riparian environment. Low–cost techniques have many

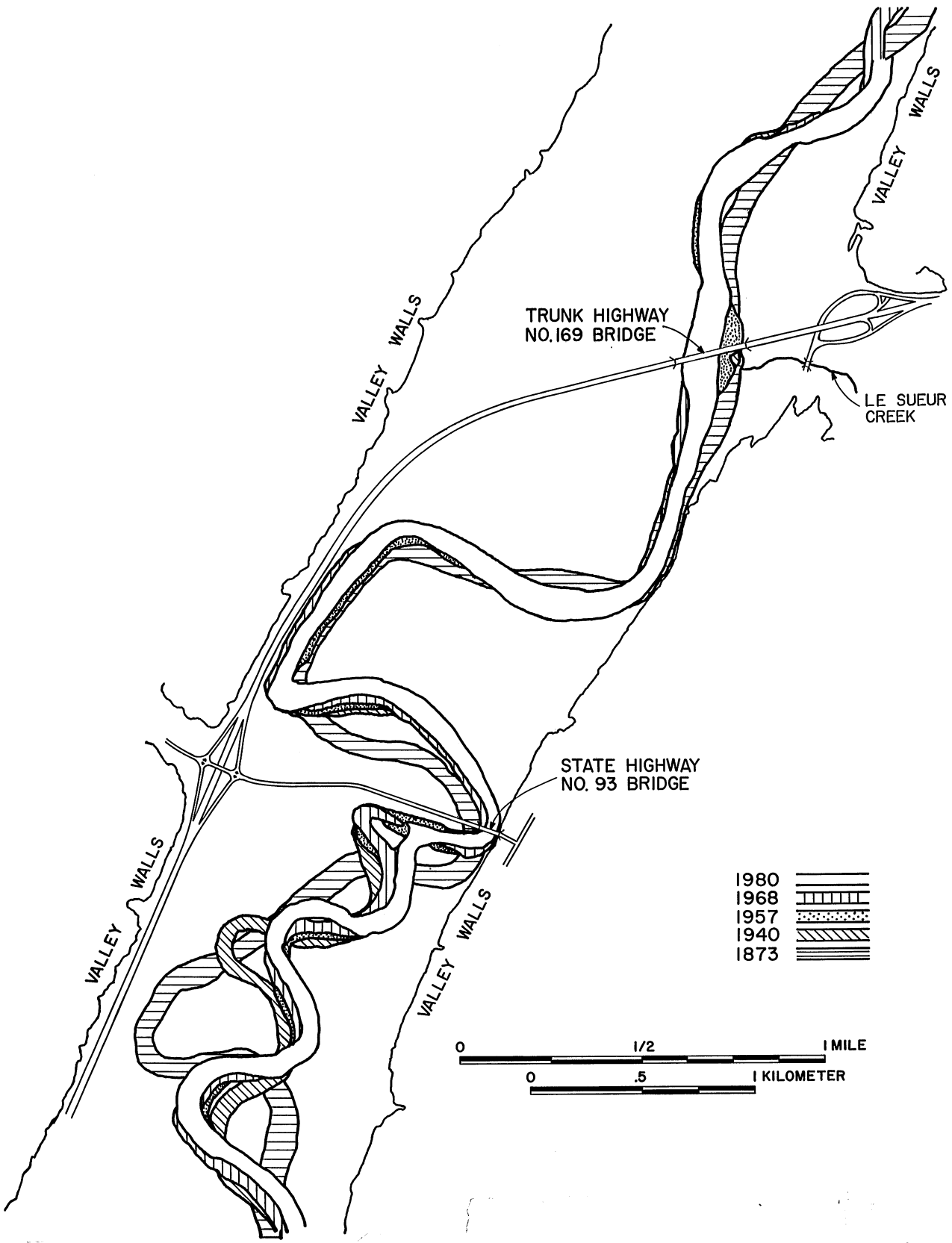

Figure 1.1 The 1873, 1940, 1957, 1968, and 1980 channels of the Minnesota River near the State Highway No. 93 bridge. Flow in the river is from bottom to top. Note the progressive tightening of the bend just upstream of the bridge. From Parker [1982].

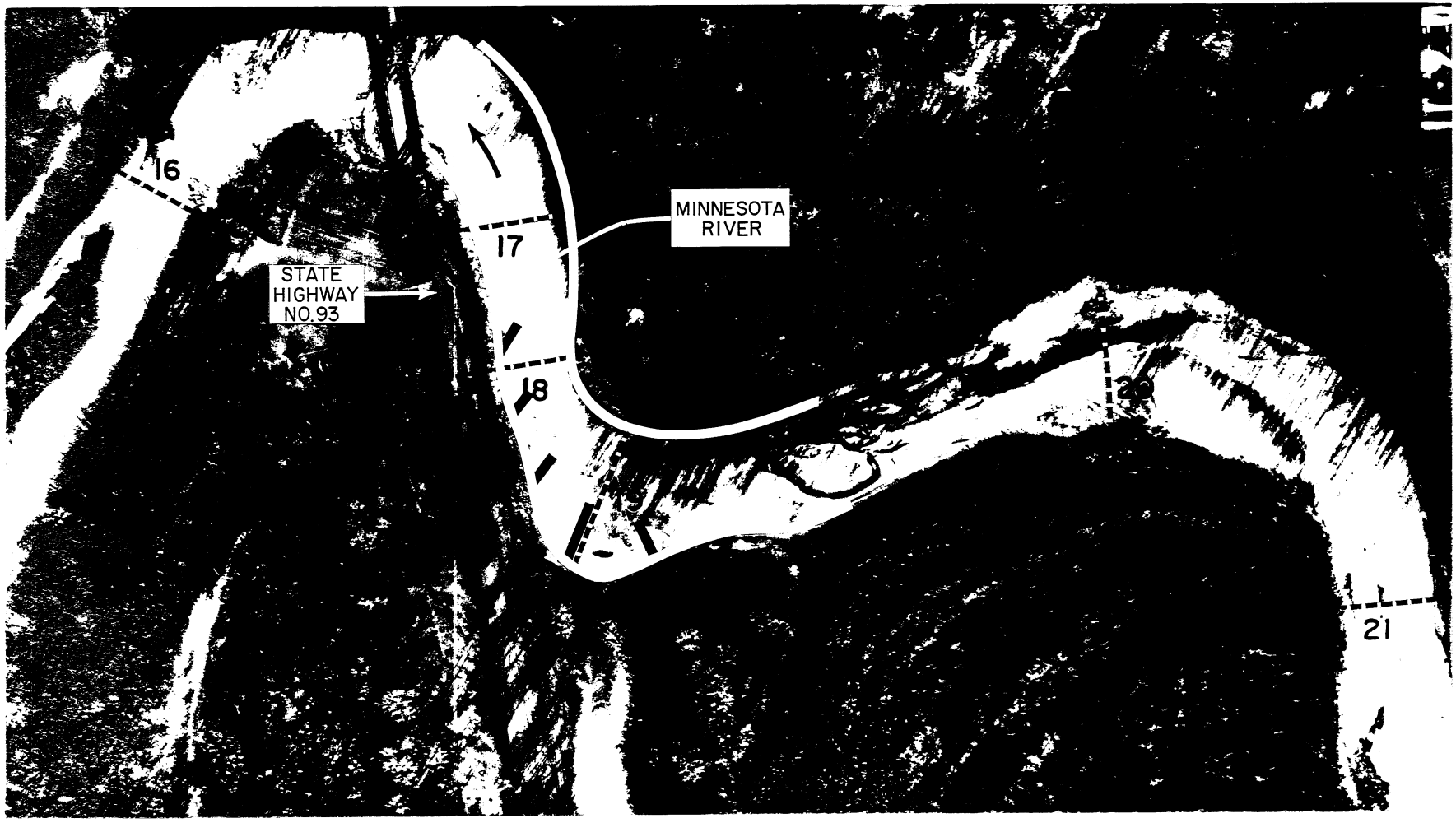

Figure 1.2 Schematic diagram for placement of rock spur dikes for protection of the western approach to the State Highway No. 93 bridge. From Parker [1982].

Figure 1.3 View of two of the rock spur dikes actually installed on the Minnesota River just upstream of the State Highway No. 93 bridge.

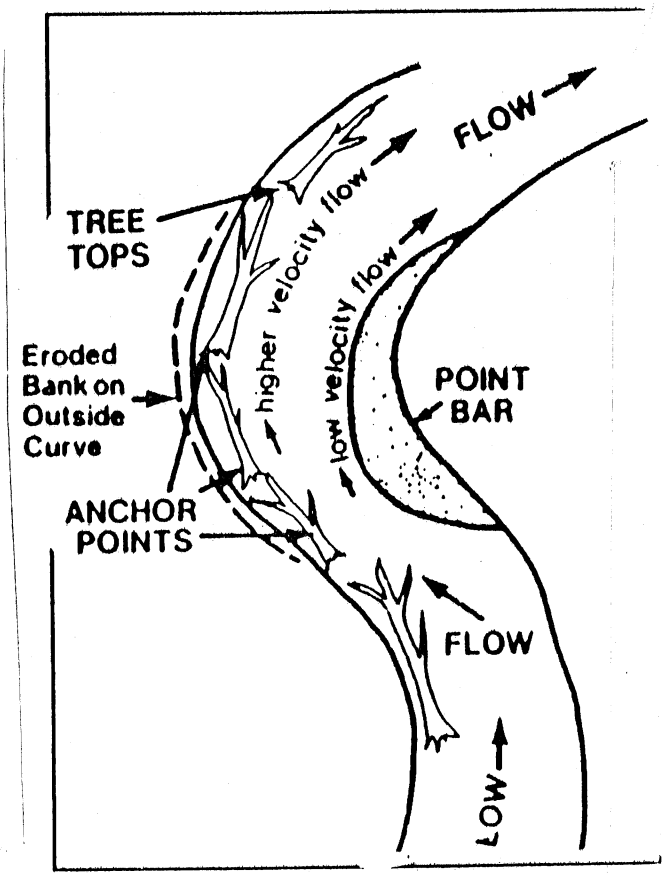

Figure 1.4 Schematic diagram illustrating the Palmiter method, according to which felled trees are used for bank protection. From Bentley, Parker, and Leuthe [1991].

applications in rural areas in Minnesota. They have the added advantage of being flexible and localized, which makes them appropriate for limited use in urban areas as well.

The present experimental study is focused upon a class of low–cost bank protection techniques that use the concept of distributed drag. A characteristic example of such a technique is the Palmiter method (Bentley, Parker, and Leuthe, 1991). The method is illustrated in Figure 1.4. Felled trees are tied to an eroding bank. The trees are left with their branches and canopy intact. During flood flow, the trees are inundated. They serve to deflect part of the flow away from the eroding bank. The remaining near–bank flow has a reduced velocity, resulting in the reduction or elimination of bank erosion. An added benefit is the tendency for sediment to accumulate in zones of low flow velocity. As a result, in some cases the eroded bank can actually be reconstructed.

Two other examples of distributed drag techniques include permeable dikes (Figure 1.5) and jacks (Figure 1.6). Both these figures were taken from Committee on Channel Stabilization (1963). These relatively low–cost structures are normally set in fields consisting of many units. By lowering the flow velocity near river banks, they can often cause significant bank deposition. In Figure 1.7, part of a permeable dike field placed along the eroding bank of a river in Indonesia is illustrated. The dikes have caused so much deposition that they have been partially buried. The newly–created land is under cultivation. It can be seen in the figure that farther downstream, where no dikes have been placed, bank erosion continues unabated.

The purpose of the present experimental study is to study bank erosion and its prevention by distributed drag techniques in the laboratory. In order to analyze a fairly tractable case, only straight channels have been considered. The experimental setup allows for the modeling of both major modes of sediment transport, bedload and suspended load. Bedload sediment tends to creep along the bed in response to local shear stress. Suspended load is carried in the water column and is available for deposition within fields of distributed drag.

The type of distributed drag selected here for further study is that associated with permeable dike fields. This case was selected because it is easy to model in the laboratory, and because the experimental results can be quantified in a consistent way. The results obtained by the study can, however, be interpreted in terms of other distributed drag techniques, including the Palmiter method.

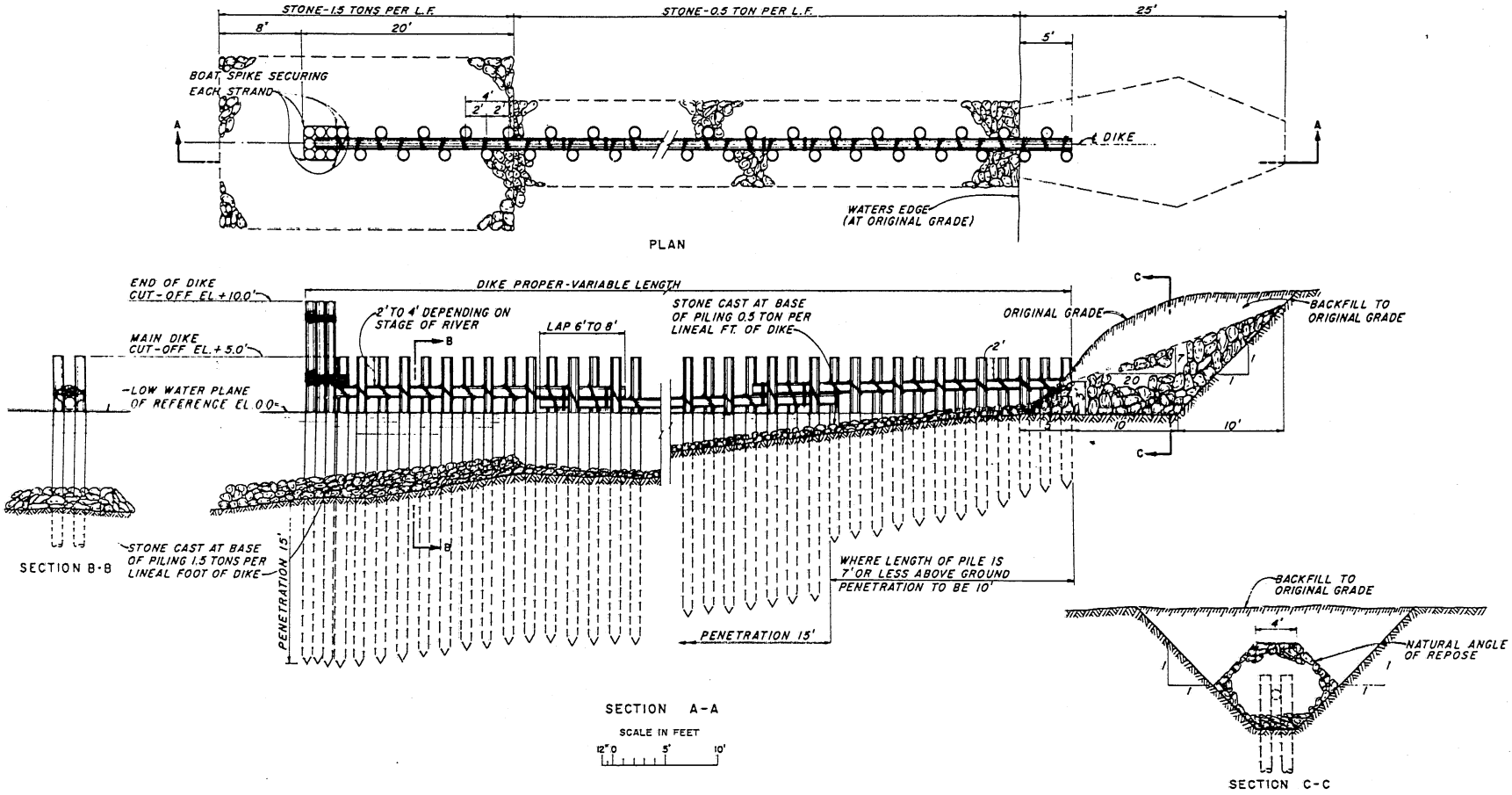

Figure 1.5 Schematic diagram of a permeable dike constructed from timber piles. These are normally used in fields of more than one dike. From Committee on Channel Stabilization [1963].

Figure 1.6 Schematic diagram of a Kellner jack. These are normally used in fields of tied jacks. From Committee on Channel Stabilization [1963].

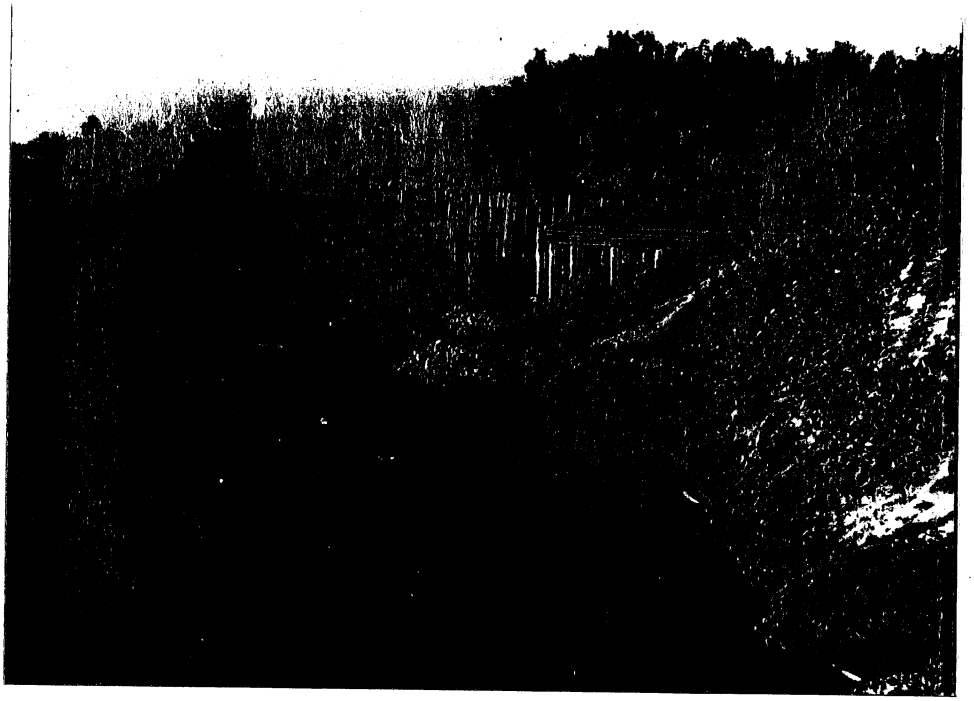

Figure 1.7 Photograph of a permeable dike field in Indonesia which has induced heavy deposition of suspended sediment. Farther downstream, the unprotected bank continues to erode. Photograph courtesy V. J. Galay.

1.2 BACKGROUND

Alluvial rivers form their channels through the interaction of flowing water and a mobile boundary. Thus a question arises as to how a stable channel is self–formed so that the available bed material is transported without an alteration of cross section. This gives rise to an interesting scientific problem, for which the shape of the boundary as well as the flow field must be determined. The stable channel problem also possesses important design aspects, which relate to how river alignment can be maintained with a minimum amount of engineering interference.

Due to the complexity of the phenomenon and the mathematical difficulty of solving it, earlier studies on this subject have been limited to empirical works, such as treatment of hydraulic geometry (e.g. Leopold and Maddock, 1953). The first mechanistic models are probably due to Glover and Florey (1951) and Lane (1955), in which the channel cross section was determined assuming that the sediment cannot be suspended and is at the threshold of motion everywhere. However, the analysis is found to be generally applicable to neither natural rivers nor laboratory flumes in that it predicts vanishing bed load transport and a much smaller width than observed. Experiments on the stable channels in coarse noncohesive sands were made by Wolman and Brush (1961), and they showed that the concept of static equilibrium is not realistic. There exists a dynamic equilibrium for which the sediment is actively transported at least in the central bed region and bed load vanishes in the side regions, so that sediment transport occurs without channel widening.

Hirano (1973) successfully treated the widening process of gravel rivers from considerations of bed load transport. However, the theory fails to predict the stable channel width for a channel with a nonvanishing load. According to the theory, as long as bed load transport exists in the central bed region, some grains in the bank region must also be in motion, since the bed shear stress must be above the critical value somewhere in the bank region. Any moving grain on the bank region is subject to not only downstream pull due to the flow, but also a transverse gravity pull due to the lateral inclination of the bank. Grains thus move down the bank region to the central bed region, causing bank erosion. Thus the channel widens indefinitely as long as a finite load is imposed. Bed load transport on the central bed region or anywhere else seems to be incompatible with a stable channel.

Parker (1978a) termed this apparent incompatibility the "stable channel paradox," and resolved the problem based on lateral momentum transfer due to turbulence. Eddy diffusion due to turbulence induces a net lateral transport of longitudinal fluid momentum from regions of high momentum to regions of low momentum, which yields a lateral redistribution of bed shear stress. Ikeda et al. (1988) have included the sediment gradation in an analysis which is similar to Parker's. A series of laboratory experiments were performed to test their analysis; the laboratory data were found to support the theory.

Charlton et al. (1978) and Andrews (1984) observed hydraulic geometry of natural gravel rivers in Great Britain and Colorado, U.S.A., respectively. An interesting finding of their field observations is that bank vegetation increases channel depth and decreases channel width. This finding is in accord with the concept of bank protection induced by distributed drag; in this case it is the bank vegetation itself that provides the drag elements. Ikeda and Izumi (1990) applied the concept of the dynamically stable channel to the case with bank vegetation, and succeeded in illustrating that bank vegetation renders the channel deeper and narrower. According to their analysis, the distribution of bed shear stress for rivers with bank vegetation is different from that without bank vegetation. Bank vegetation enables the bank to be steeper, and moves the point at which critical Shields stress is realized to deeper water. This results in a deeper and narrower channel.

The implication here is that permeable dikes, which have a function similar to bank vegetation, can act in an analogous way to protect against bank erosion.

When sediment fine enough to be suspended is largely absent from a channel, the maintenance of stable banks requires that the grains composing those banks be immobile. Therefore, the key to bank protection in such cases is in either increasing grain size (riprap) or reducing boundary shear stress (e.g. distributed drag) so as to prevent motion of bank material.

In the case of a channel which includes large amounts of easily suspendable sediment such as fine sand, the mechanism of equilibrium bank maintenance is more complicated. Even if bank material is moved by bedload transport, causing a tendency toward bank erosion, this material can be replaced by deposition from suspended sediment. The material in question is transported from the central bed region to the bank region due to turbulent diffusion. As a result, the banks can still be in equilibrium, although in this case the equilibrium is a dynamic one. Parker (1978b) formulated this mechanism and obtained an equilibrium cross–sectional bed profile for sand–silt rivers. An important result is that the center depth of sand–silt rivers tends to vary as $1/\sqrt{S}$, where S denotes streamwise channel slope.

Ikeda et al. (1991) studied the effect of permeable dike on the deposition of suspended sediment. The distribution of velocity and bed shear stress was obtained theoretically, from which the distribution and deposition rate of suspended sediment in the dike field were derived. Since their analysis does not include lateral bed load and the time variation of bed profile, an equilibrium state of the channel cannot be predicted. Their analysis, however, suggests that the suspended sediment is transported from the channel center, where the suspended concentration is larger, to the permeable dike region, where the concentration is typically smaller, as would be expected. Their work also indicates that maximum deposition occurs near the boundary where the permeable dike region meets the river bank, at least in the case of a channel with initially uniform depth.

In the present research, the modeling of fluvial processes has been made as realistic as possible by allowing for both coarse bedload and fine suspended load. For this purpose, two model sediments were used. The coarser material consisted of crushed walnut shells with a specific gravity of 1.4 and a median grain size d_{c50} of 2.6 mm. The finer material was composed of vinyl chloride homo–polymer powder, with specific gravity of 1.40 and a median size d_{s50} of 0.12 mm. These lightweight materials were chosen so as to reproduce in a small–scale laboratory flume the sediment mobility characteristic of field streams.

The research described here consists of a study of five sets of experimental cases. These cases are summarized below.

Case 1: *Critical Shields stress over flat beds.* The experiments of Case 1 were directed toward determining the flow conditions at which the coarser material is mobilized. This can be quantified in terms of the concept of critical Shields stress, as outlined in the description of the experiments. The bed configuration was flat: no channel was modeled.

Case 2: *Self–formed channels with no suspended sediment and no permeable dikes.* In the course of these runs, the processes of bank erosion and channel widening were studied in the absence of bank protection. In addition, the hydraulic characteristics of the final equilibrium state, i.e. a self–formed straight channel with noncohesive coarse material, were documented and studied.

Case 3: *Self–formed channels with no suspended sediment and bank protection provided by permeable dikes.* For these studies, the initial channel was protected with various configurations of distributed drag elements before commencing the flow. The purpose of the experiments was to quantify the degree of protection against erosion provided by the permeable dikes in the absence of significant sediment suspension.

Case 4: *Self–formed channels with suspended sediment in the absence of permeable dikes.* In these experiments, the skeleton of the channel was composed of coarser material, but a continuous supply of fine, suspendable material was supplied as well. The experiments were performed to reveal how suspended sediment deposits within the channel, and how a mixed–mode state of equilibrium is achieved.

Case 5: *Self–formed channels with suspended sediment and permeable dikes.* This last set of experiments was perhaps the most important one. The effect of permeable dikes on the deposition of suspended sediment within the channel cross–section was studied. It was found that not only could bank erosion be prevented, but that significant deposition could be induced, resulting in effective channel narrowing.

1.3 EXPERIMENTAL APPARATUS AND TECHNIQUE

A 13–m long, 60–cm wide, straight laboratory channel at St. Anthony Falls Hydraulic Laboratory, University of Minnesota was used for these experiments. The slope and discharge of the flume are adjustable. The flume is shown in Figure 1.8.

Water is circulated by two pumps, a small pump and a large pump. The use of two pumps is necessitated by the need to recirculate the sediment as well as the water. The large pump is a centrifugal pump which is powered by electricity. It was used for recirculating the majority of the water and fine sediment, but none of the coarse sediment. This is because the impellers of a centrifugal pump would act to grind the crushed walnut shells, thus reducing their size.

The small pump is a diaphragm pump, operating on the same principle as a heart. It is powered by compressed air, alternately sucking fluid in and pushing it out. The rubber walls of the diaphragm prevent abrasion of the walnut shells. This pump was used thus for recirculating all of the coarse sediment as well as a small fraction of the water.

In order to segregate out the walnut shells at the downstream end of the flume, two funnels in series were provided. As water passes over the first funnel, the coarse sediment drops into a line leading to the diaphragm pump. The remaining water and fine sediment then enters the second funnel downstream, where it is led to the centrifugal pump for recirculation.

Water discharge was monitored with orifice meters set in the return line. Water elevation at the downstream end was controlled with a gate, so as not to yield significant drawdown or backwater.

As noted previously, the coarse material consisted of a well–sorted grade of crushed walnut, with median diameter d_{c50} of 2.6 mm and specific gravity of 1.406. The grain size distribution of this material is shown in Fig. 1.9. The fine material consisted of vinyl chloride homo–polymer powder, with a median grain size d_{s50} of 0.12 mm and a specific gravity of 1.4. The corresponding grain size distribution is shown in Figure 1.10.

Before commencing any of the experiments, the flume was filled with walnut shells. At the upstream end, an entrance box lined with coarse stones was provided to allow for energy dissipation of the water flowing from the return lines. At the downstream end, a sill was provided to maintain minimum channel depth. The sill was made permeable so as to allow for the evacuation of groundwater.

For Case 1, the initial bed was screeded to a flat configuration. No self–formed channel was provided. Vertical steel walls served as the channel boundaries. In the other cases, a self–formed half–channel was provided. That is, channel centerline was delineated by a vertical steel wall, leaving the bed and one bank of the half–channel completely erodible. The motivation for doing this is the suppression of meandering tendencies

Figure 1.8 View of the tilting flume at Saint Anthony Falls Hydraulic Laboratory used for the experiments, looking upstream.

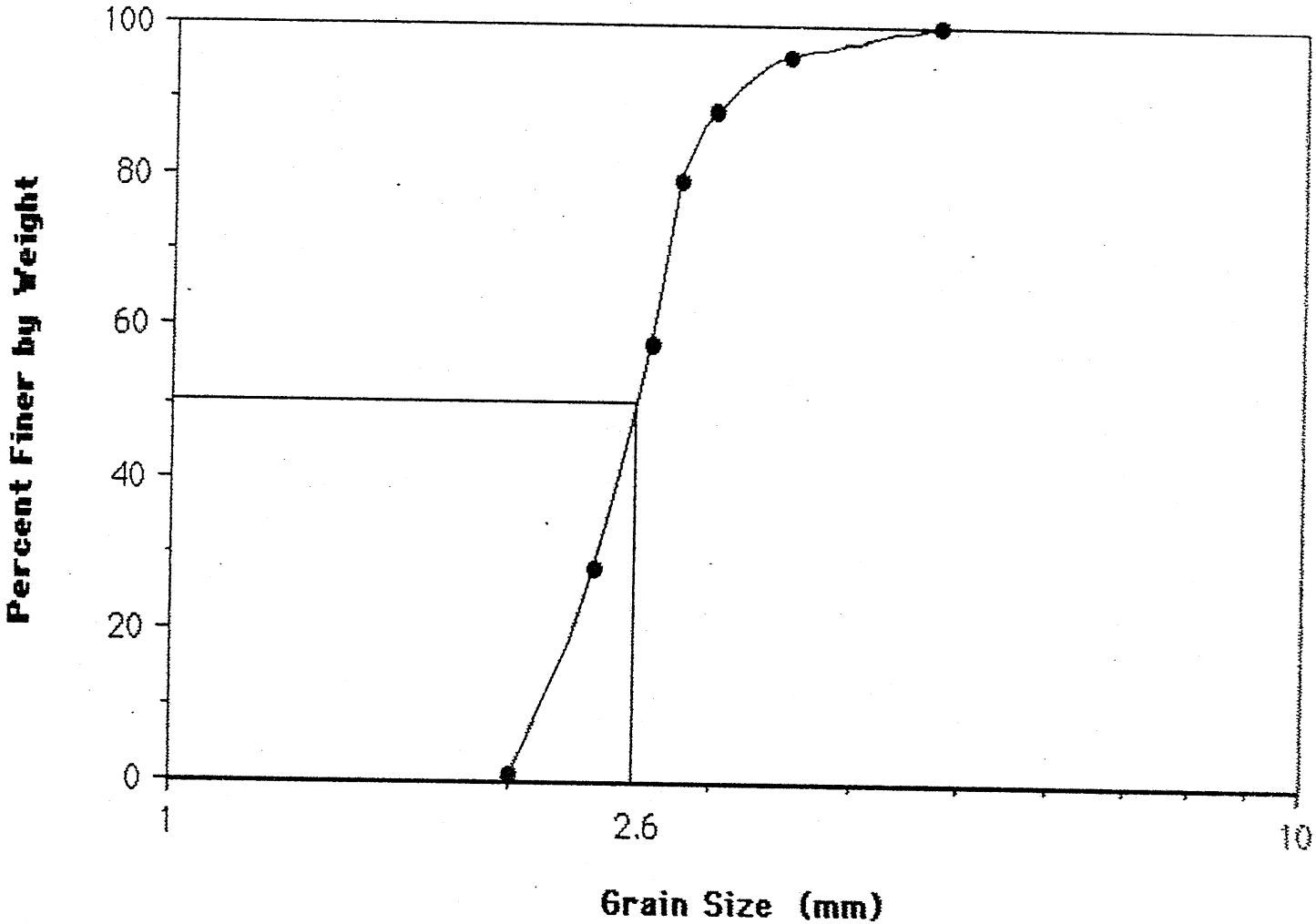

Figure 1.9 Grain size distribution of the walnut shells used in the experiments as coarse material subject to bedload transport.

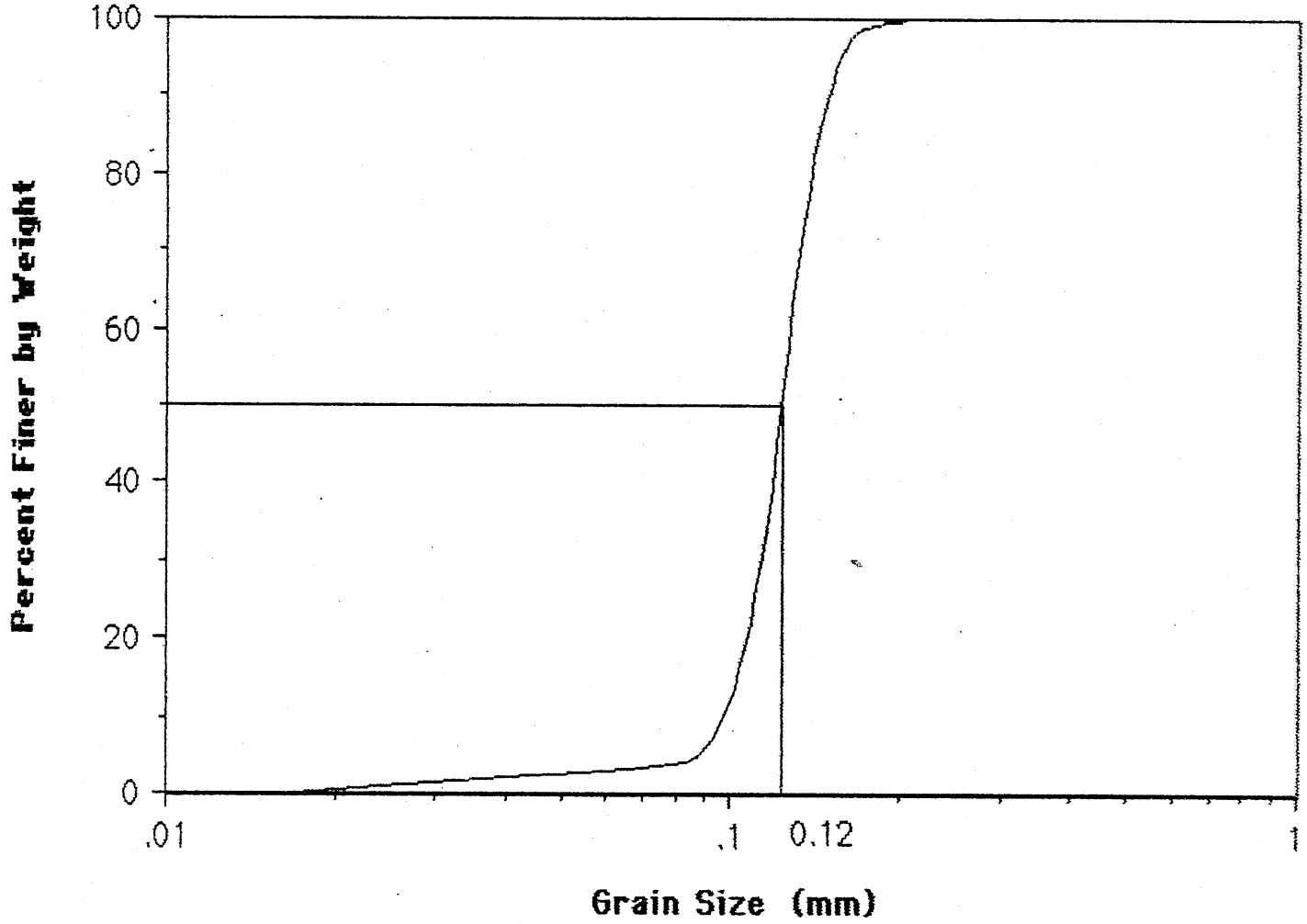

Figure 1.10 Grain size distribution of the plastic (vinyl chloride homo–polymer) particles used in the experiments as suspendable fines.

associated with wide channels (Ikeda, 1981). In the present experiments, meandering tendencies are an undesirable complication. The initial cross–section was molded into a trapezoidal shape with a template.

Water discharge was measured with an orifice meter in the return line connected to the centrifugal pump, and with an elbow meter in the return line connected to the diaphragm pump.

Bed and water surface elevations were recorded with a standard point gage. The data so taken were used to determine channel cross–sectional shape as well as longitudinal water surface and bed slopes. For the purpose of measurement, an (x, y, z) coordinate system was set up such that x represents the streamwise distance from the entrance box, y represents the transverse distance from the vertical steel wall, and z represents vertical distance from an arbitrary datum. Reference is made to this coordinate system in many of the figures that follow.

In several of the experiments, flow velocities were measured with the aid of a 3 mm micropropeller velocimeter (Shinozuka). In addition, for several runs with suspendable material, concentrations of suspended sediment were determined by either analyzing samples siphoned from the flow, or with the use of an optical turbidimeter (Kenek).

A bypass in the line connected to the diaphragm pump allowed for determination of bedload transport rates. Water from the line could be diverted into a settling tank, allowing the walnut shells to settle into a vertical pipe of one inch in diameter. The pipe was made from clear plastic in order to allow for visibility. The volume transport rate of walnut shells was determined by measuring the accumulation time in the plastic pipe.

A brief summary of experimental procedure follows. More details are provided in the following sections.

Case 1: *Critical Shields stress over flat beds.* In this case, the bed was screeded completely flat. No suspendable fines were introduced. The channel was filled with water at vanishing streamwise slope. The flow discharge was slowly increased to 2 ~ 3 liters/s. The bed slope was then gradually increased until the walnut shells were noted to be in motion. Adjustments were made to the tailgate setting until backwater effects were eliminated, resulting in a water surface sloping parallel to the bed in the streamwise direction.

Flow conditions were then measured to define the hydraulic conditions at the onset of significant motion. The criterion for determining whether the bed was in motion was, of necessity, partly subjective.

Case 2: *Self–formed channels with no suspended sediment and no permeable dikes.* The flume was molded into an initial channel with a relatively narrow trapezoidal shape. No fines were introduced. The channel was filled with still water before the start of experiments. The pumps were then turned on, and the discharge of recirculated water was gradually increased. The elevations of the free surface and the bed were measured

with the point gage at cross–sections located 5 meters and 8 meters from the entrance box. These measurements served as the basis for determining the time change in cross–sectional shape. This measuring reach was chosen so as to obtain a channel with width and depth that were relatively uniform in the streamwise direction, and unaffected by entrance and exit effects.

At the same time, the channel width and water surface and bed elevation were measured every 1 m in the streamwise direction along the entire length of the channel. These measurements formed the basis for determining the streamwise variation of channel center depth, as well as longitudinal bed and water surface slope. The bedload transport rate of walnut shells was measured with the use of the bypass device described above.

The intent was to continue each run until a final equilibrium channel section was obtained. This final mobile–bed equilibrium in the absence of bank erosion was achieved in the case of several runs; in several others, irregularities such as the formation of meandering tendencies necessitated the early termination of the experiment.

Case 3: *Self–formed channels with no suspended sediment and bank protection provided by permeable dikes.* The procedure for these experiments was similar to Case 2. The major difference was in the installation of model permeable dikes near the banks.

In the field case, permeable dikes are typically constructed from rows of timber piles, as shown in Figure 1.5. To model this in the laboratory, wire screen was used. One of these screens is shown in Figure 1.11. The diameter of the wire from which the screens were constructed is 1.65 mm. The mesh is square, with a mesh size (from wire center to wire center) of 11.8 mm. Each piece of screen was 31 cm long and 12.5 cm wide.

These screens were imbedded into the bank immediately after screeding, and before the commencement of the flow. Care was taken so as not to disturb the bank slope at the time of installation. The screens were installed perpendicular to the channel itself, with a set streamwise spacing for the length of the flume. A typical setting is shown in Figure 1.12. In a typical case, screens were placed from $x = 0$ (entrance box) to $x = 9$ meters.

Each run was then commenced in a manner similar to Case 2. The measuring sections for cross–sectional data were chosen to be 5 and 7 meters from the entrance box.

Case 4: *Self–formed channels with suspended sediment in the absence of permeable dikes.* The experimental procedure was identical to that of Case 2 up to the attainment of a final steady state with no further bank erosion. No fines were introduced until this final state was achieved. Cross–sectional data were taken at sections located 5 and 7 meters downstream of the entrance box.

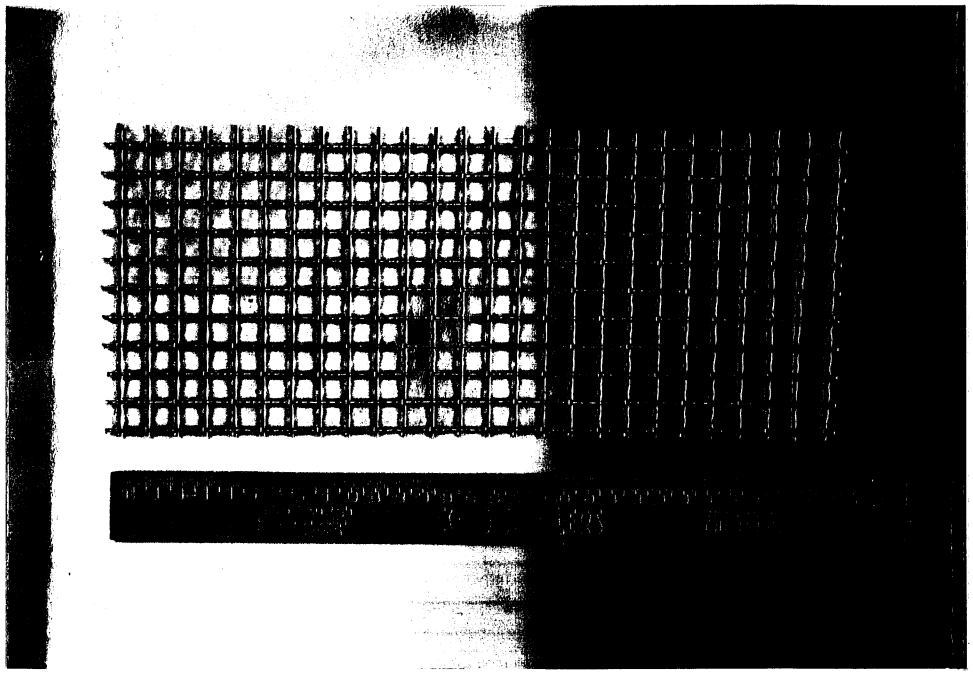

Figure 1.11 Photograph of one of the screens used as model permeable dikes. The scale on the ruler is in centimeters.

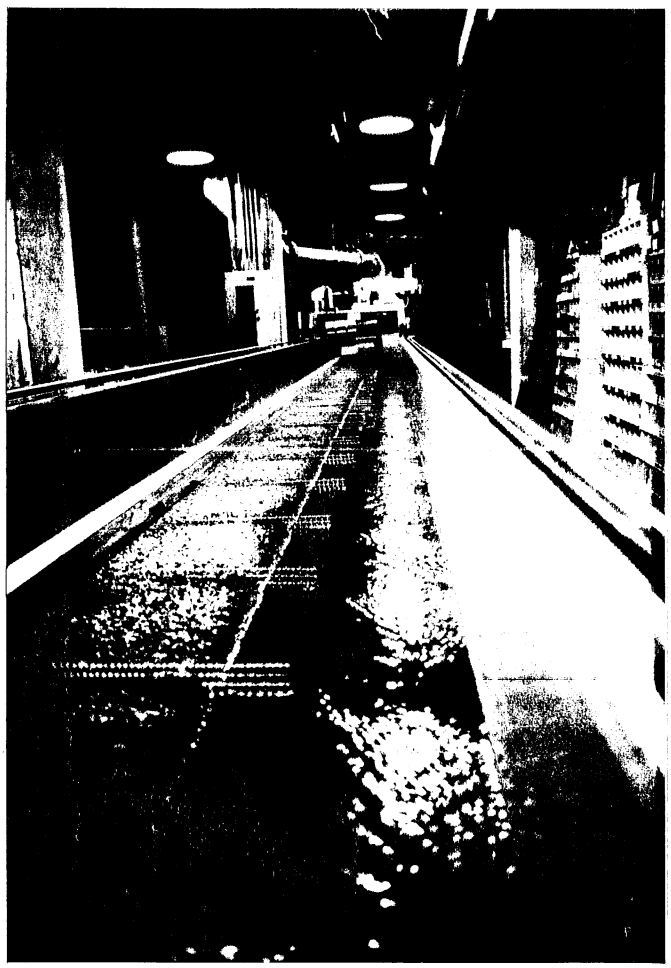

Figure 1.12 Photograph illustrating the placement of permeable dikes. The view is of Run 14, looking upstream.

Once the final state without fines was documented, a slurry of fines and water was gradually introduced from the downstream end of the flume into the recirculating lines connected to the pumps. At the same time, water was removed from the channel so as to conserve the total amount of water in the system.

The fines tended to settle into the pores of the walnut shells in time, eventually reaching a new steady state. In a typical case, at this steady state the surface layer of walnut shells remained essentially exposed in some parts of a given cross–section, but became completely covered with fines in other parts.

The propeller meter was used to measure the cross–sectional distribution of streamwise flow velocity. The distribution of suspended sediment concentration on a cross–section was measured using one of two methods. The first of these is siphoning, and the second involves the use of an optical turbidimeter.

After these measurements were complete, the pumps were turned off and the channel drained carefully so as not to disturb the deposit of fines. The measuring cross–sections were re–surveyed so as to reveal the pattern of deposition of fines over the walnut shells.

Case 5: *Self–formed channels with suspended sediment and permeable dikes.* The experimental procedure was identical to that of Case 3 until the attainment of a final equilibrium state in the absence of fines. Subsequent to this, fines were added, and the experiment proceeded according to the method outlined for Case 4.

1.5 EXPERIMENTAL RESULTS

A summary of the experiments performed for Cases 2 ~ 5 is provided in Table 1. In Table 1, the water discharge Q is listed for each run, along with the following values determined at the end of the run when an approximate equilibrium had been achieved: streamwise slope S, water surface width B, and depth D_c in the center region of the channel. Also included is information concerning the placement of permeable dikes, as well as whether or not a supply of suspendable fines was introduced. Only a selection of experimental results are reported herein. A complete compilation of experimental results can be found in an Appendix [Appendix, Project Report No. 320, SAFHL, Compilation of Experimental Results of Studies of Bank Erosion in Rivers and Its Prevention by Low–Cost Means, September 1991].

In Cases 2 and 3, the experiments were continued to final equilibrium without the addition of fines. In Cases 4 and 5, the runs were first continued to final equilibrium without fines, and then continued to a new equilibrium with fines. The data in Table 1 for width B and center depth D_c pertain to the equilibrium without fines, regardless of the case in question.

The experiments for Case 1 were of a simple nature, and are thus not tabulated in that table.

Table 1. Summary of Laboratory Data

Run No.	Case	Q cm^3/s	S $\times 10^{-3}$	D_c, cm	B , cm	permeable dike	suspended sediment
1	2	1390	1.74	2.61	27.7	none	none
2	2	1280	2.70	2.25	30.5	none	none
3	2	1400	2.30	2.56	26.5	none	none
4	2	1370	2.20	2.59	27.3	none	none
7	2	3320	0.99	4.28	36.8	none	none
8	2	3310	1.20	4.74	34.9	none	none
9	2	3500	1.35	4.26	38.0	none	none
10	2	790	3.00	2.10	19.9	none	none
11	2	820	2.40	2.39	18.8	none	none
12	2	860	2.80	2.44	19.6	none	none
14	3	3200	1.35	4.89	30.0	$B_c > 22$ cm, $L = 40$ cm	none
15	3	3600	2.05	5.45	32.0	$B_c > 22$ cm, $L = 40$ cm	none
16	3	4380	1.34	4.82	33.5	$B_c > 22$ cm, $L = 80$ cm	none
17	2	3048	1.19	4.02	34.5	none	none
18	4	1087	2.67	2.32	23.0	none	added
19	4	760	3.16	2.26	32.0	none	added
20	4	not measured	2.16	2.30	33.5	none	added
21	5	1031	2.70	3.09	19.0	$B_c > 12$ cm, $L = 40$ cm	added
22	5	1115	3.86	3.10	20.5	$B_c > 12$ cm, $L = 40$ cm	added
23	5	3461	1.70	5.36	31.0	$B_c > 22$ cm, $L = 40$ cm	added
24	5	3004	1.80	4.70	30.0	$B_c > 20$ cm, $L = 40$ cm	added
25	5	980	3.02	2.30	19.0	$B_c > 12$ cm, $L = 25$ cm	added
26	5	1053	3.50	2.90	20.0	$B_c > 9$ cm, $L = 75$ cm	added
27	3	1199	3.65	2.90	20.0	$B_c > 12$ cm, $L = 40$ cm	none
28	4	not measured	1.00	4.88	33.0	none	added

Note: For cases 3 and 4, the depth D_c and width B correspond to the final stable state before the addition of fines.

Case 1: *Critical Shields stress over flat beds.* Care was taken so as to achieve normal flow conditions at the onset of motion. This allowed for the determination of a critical bed shear stress τ_{cr}, where

$$\tau_{cr} = \rho g D S \tag{1–1}$$

Here D and S denote the observed flow depth and slope at the onset of motion: ρ denotes the density of water and g denotes the acceleration of gravity.

The experimental values for critical bed shear stress were placed in standard Shields dimensionless form. That is, τ^*_{cr} denotes the critical Shields stress, where

$$\tau^*_{cr} = \frac{\tau_{cr}}{\rho R g d_{c50}} \tag{1–2}$$

In the above relation R denotes the submerged specific gravity of the sediment, given by $(\rho_s - \rho)/\rho$. In the case of the walnut shells, R tables a value of 0.41.

Several experiments were performed. The data displayed a certain amount of scatter due to the subjective nature of the criterion for the onset of significant motion of bed grains. An approximate value of τ^*_{cr} of 0.04 could nevertheless be determined, based in estimates ranging from 0.033 to 0.047.

Case 2: *Self–formed channels with no suspended sediment and no permeable dikes.* The relevant experiments are Runs 1 ~ 12 and 17. Not all of the experiments were successful in the sense that a spatially uniform final equilibrium state was achieved. Runs 4, 8, and 11 provide representative examples of successful runs, and are discussed in more detail here. Of the various initial cross–sections used in all the runs of Case 2, Run 11 had the narrowest, Run 8 had the widest, and Run 4 was intermediate between these two extremes.

Recall that only a half–channel is modeled in the experiments, so that the cross–section is demarcated by an erodible bank on one side and a vertical steel wall at the channel "center". In all cases, the initial channel was screeded to be trapezoidal with a side slope of 30° along the erodible bank, as shown in Figure 1.13. The erodible bank joined to an elevated region, screeded flat, also consisting of erodible walnut shells. The initial channel depth, i.e. the depth from the channel bottom to the top of the erodible bank, was always set to be larger than the initial depth of flow in the channel.

The initial channel of Run 4 had a top–bank width of 20 cm, a depth of 4 cm, and a bottom depth of 13 cm. The flow discharge Q was

held at 1.37 liters/s throughout the run. The experiment continued for 7 hours, by which time it was deduced from cross–sectional measurements that a dynamic equilibrium had been essentially achieved.

The initial channel of Run 8 had a top–bank width of 30 cm, a depth of 6 cm, and a bottom depth of 20 cm. The flow discharge Q was 3.31 liters/s. An approximate stable dynamic equilibrium was attained after 6 hours and 45 minutes of run time.

A typical view of a run in progress corresponding to Case 2 is shown in Figure 1.14.

The initial channel of Run 11 had a top–bank width of 15 cm, a central depth of 3 cm, and a bottom depth of 10 cm. The flow discharge Q was 0.82 liters/s. An approximate stable dynamic equilibrium was attained after 4 hours of run time.

Figures 1–15a ~ 1–15c document the time evolution of flow center depth D_c. Here D_c denotes the depth from the water surface to the bed in the essentially flat center region of the channel, away from either the eroding bank of the opposing vertical steel wall. The plots are expressed in dimensionless form. Dimensionless center depth D_c^* is defined as

$$D_c^* = \frac{D_c}{D_{ci}} \tag{1–3}$$

where D_{ci} denotes the initial flow depth in the center region of the channel. Dimensionless time t* is defined as

$$t^* = \left(\frac{Rg}{d_{c\,50}}\right)^{1/2} t \tag{1–4}$$

where t denotes dimensioned time.

It is seen on all three figures that center depth tended to decrease in time, first rapidly and then tapering off toward a final steady state. The increase in center depth is due to bank erosion. Lateral bedload down the bank slope results in the transport of eroded bank material to the center region of the channel, where it is deposited. The result is an increase in bed elevation in the center region of the channel, and an associated decrease in depth.

The water surface width of the half–channel is denoted as B; this can be non–dimensionalized into the form

$$B^* = \frac{B}{B_i} \tag{1–5}$$

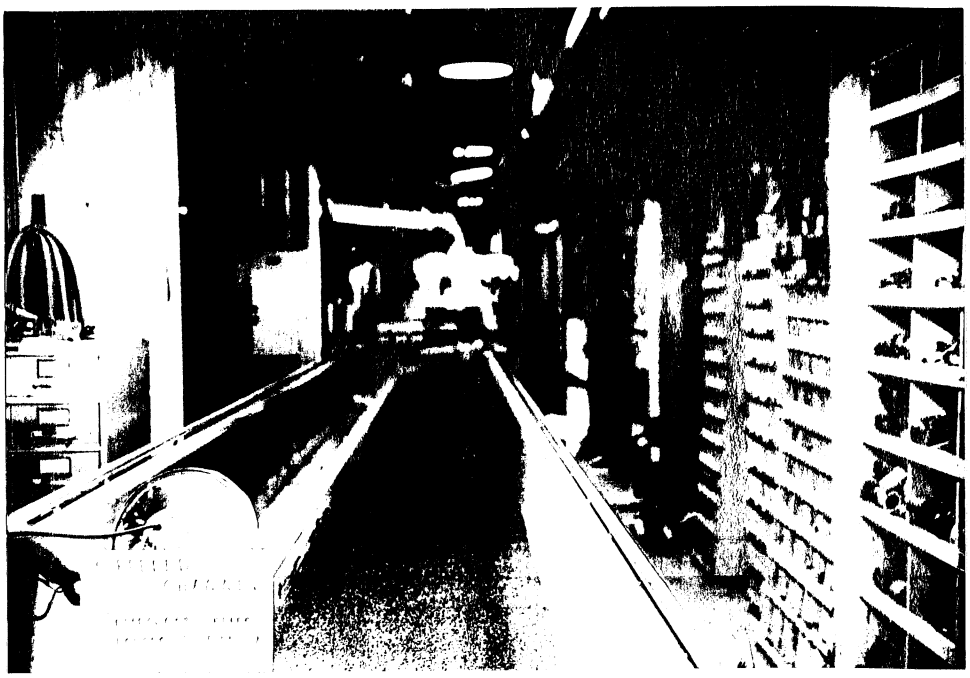

Figure 1.13 Photograph illustrating the initial narrow trapezoidal cross–section used for the runs. The view is looking upstream.

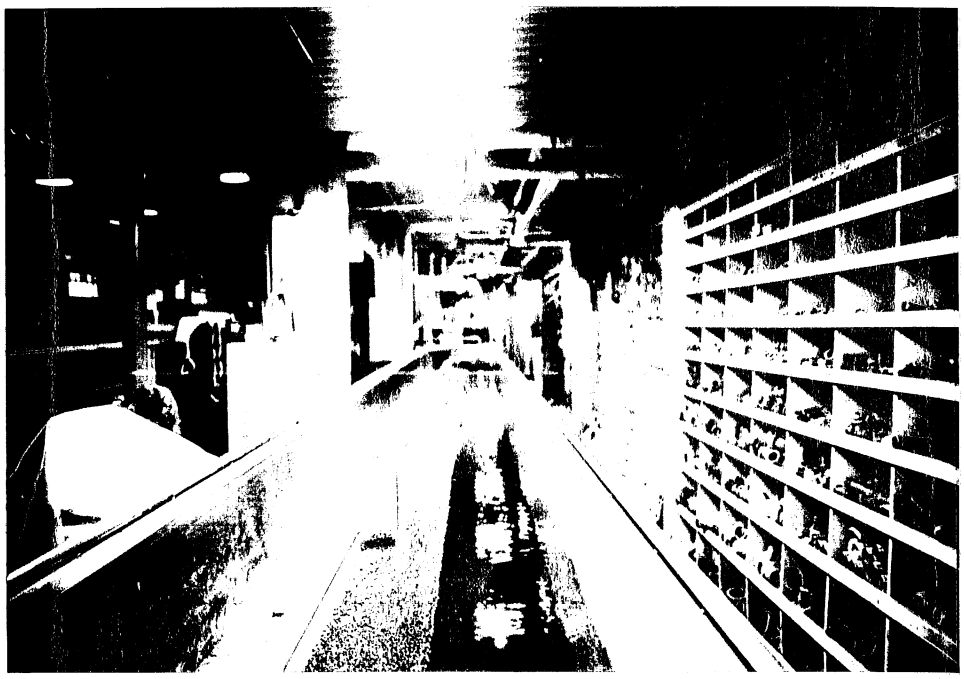

Figure 1.14 Photograph illustrating a typical run corresponding to Case 2, for which neither permeable dikes nor fines were introduced. The view is looking upstream.

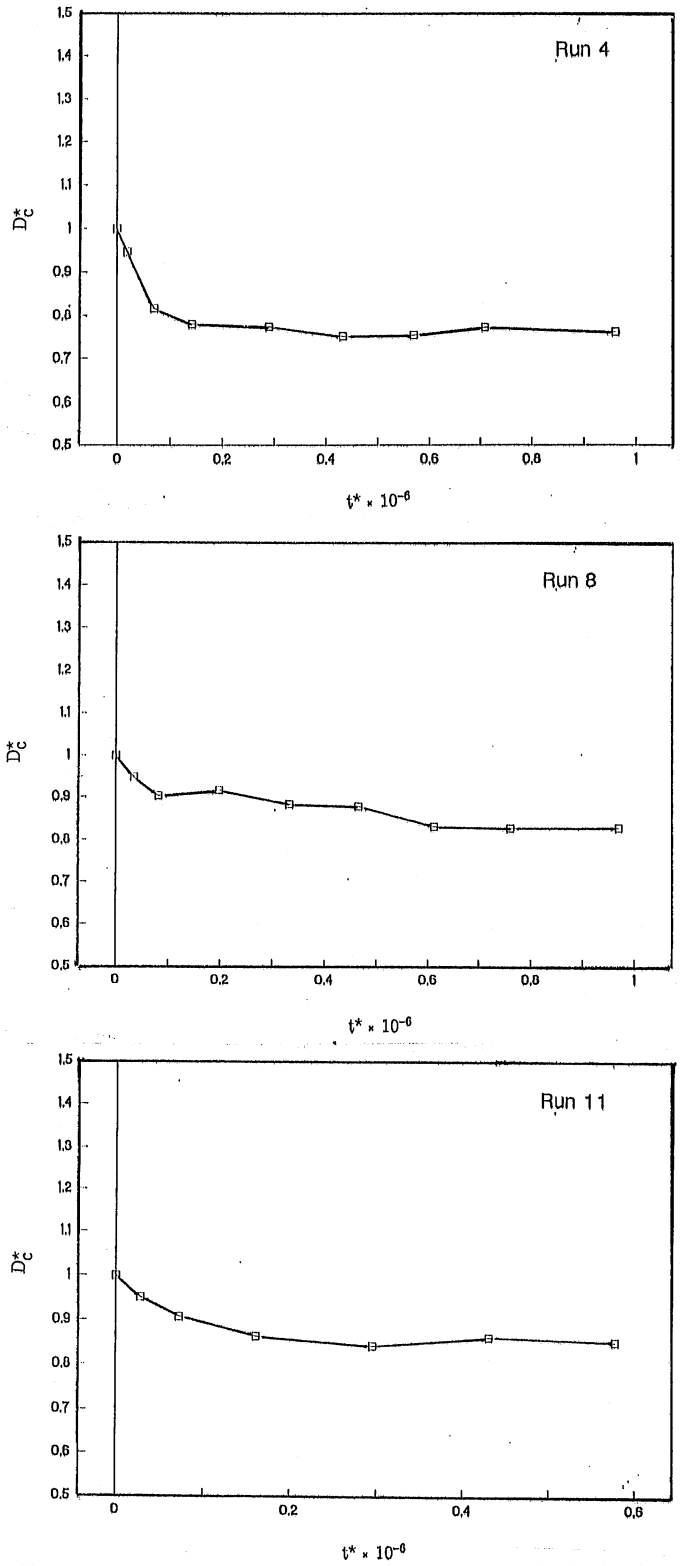

Figure 1.15 Time variation of dimensionless center depth D_c^* versus dimensionless time t^* for three runs corresponding to Case 2. a) Run 4, b) Run 8, c) Run 11

where B_i denotes the initial water surface width. The time variation of width is documented in Figures 1–16a ~ 1–16c for the three runs in question. Width initially increases rather rapidly as bank erosion proceeds, but then tends slowly toward a constant equilibrium value.

The Shields stress in the center region of the channel τ_c^* can be computed with the aid of (1–1) as follows:

$$\tau_c^* = \frac{D_c S}{R d_{c50}} \tag{1–6}$$

Plots of τ_c^* versus t^* for the three runs in question are provided in Figures 1–17a ~ 1–17c. The overall tendency is a decline toward a final equilibrium value that is probably somewhat less than 0.053. This value exceeds the estimated value of critical Shields stress τ_{cr}^* of 0.04 by about 30 percent, suggesting that even at the final equilibrium, when bank erosion ceases, streamwise bedload transport in the center region of the channel does not vanish. The existence of a non–vanishing bedload transport at the end of each of the three runs was confirmed visually.

The process of bank erosion, as well as deposition in the central region of the channel, is documented in the cross–sectional profiles of Figures 1–18a ~ 1–18c. In all three runs, the cross–section is seen to evolve from an initially narrow, trapezoidal shape to a wider, shallower profile. The central region of the channel, away from either the erodible bank or the vertical steel wall, tends to become flat in the transverse direction. The bank region tends to a gently curving smooth profile.

The process of bank erosion was observed to proceed particle by particle rather than in terms of overall slope failure. The bank slope at the water margin was found to be close to the angle of repose for submerged walnut shells.

In Figures 1–19a ~ 1–19c, the profiles of the previous three figures have been normalized in terms of center depth D_c and water surface width B at the time. When plotted in this fashion, it can be seen that the final normalized profiles for all three runs are essentially identical. This suggests the possibility of a universal equilibrium profile for the river type under consideration.

Case 3: *Self–formed channels with no suspended sediment and bank protection provided by permeable dikes.* Runs falling into this category include Runs 14, 15, 16 and 27. The parameters L and B_c used to set the permeable dikes are illustrated in Figure 1.20: L denotes the streamwise spacing, and B_c denotes the width of the central portion of the channel between the vertical steel wall and the tip of the dikes. A photograph illustrating the setting is provided in Figure 1.12.

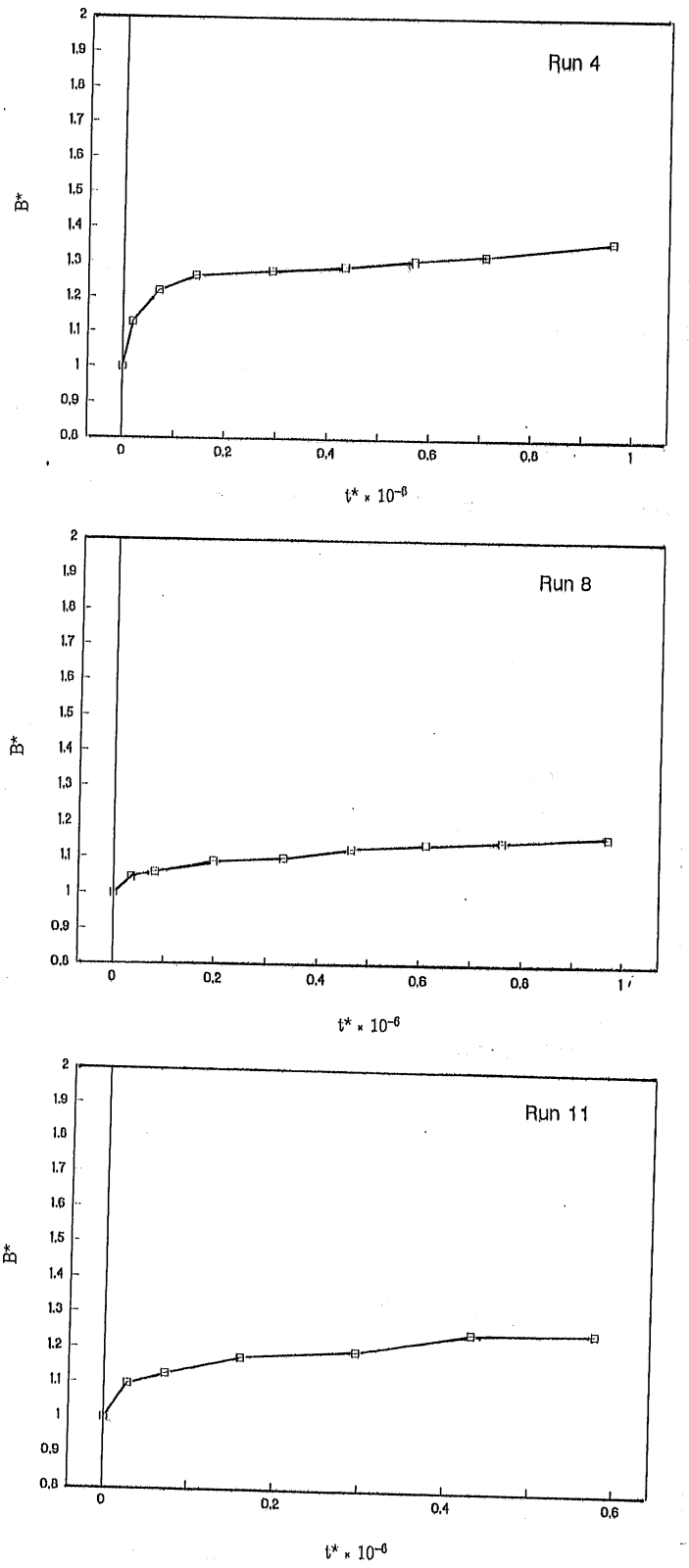

Figure 1.16 Time variation of dimensionless water surface width B^* versus dimensionless time t^* for three runs corresponding to Case 2. a) Run 4, b) Run 8, c) Run 11

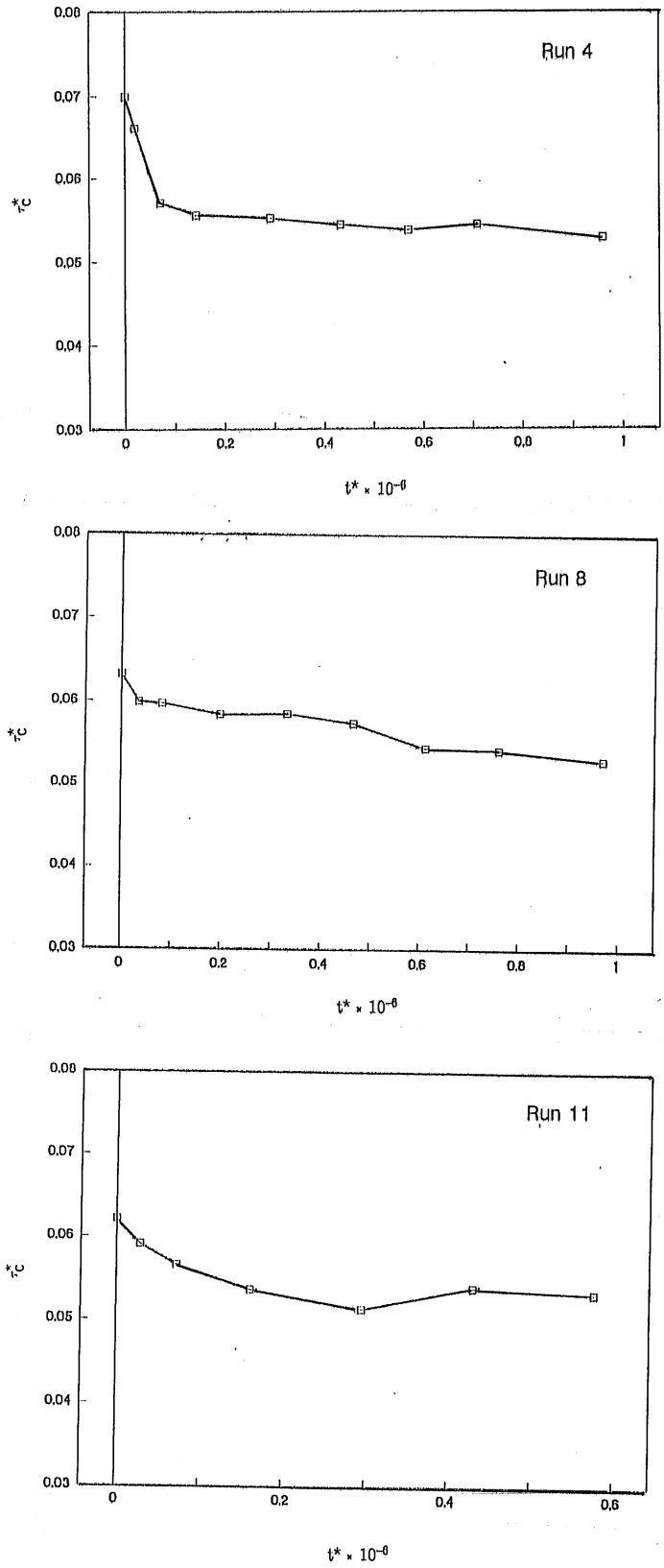

Figure 1.17 Time variation of channel center Shields stress τ_c^* versus dimensionless time t^* for three runs corresponding to Case 2. a) Run 4, b) Run 8, c) Run 11

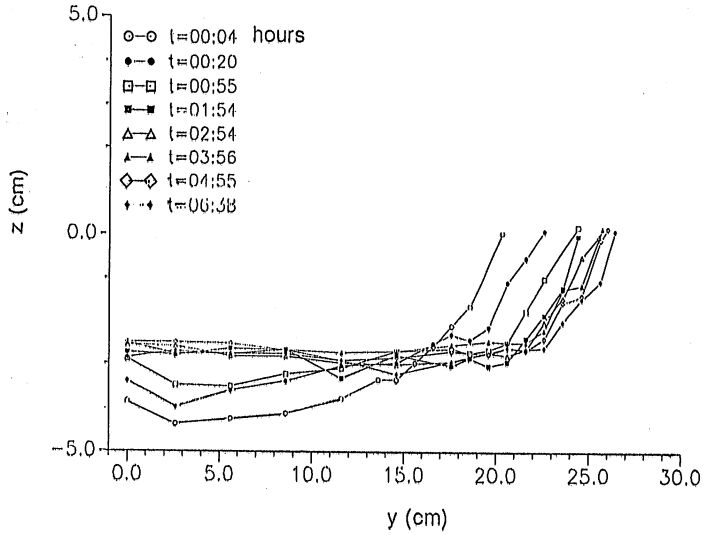

Run 4 x = 8 m

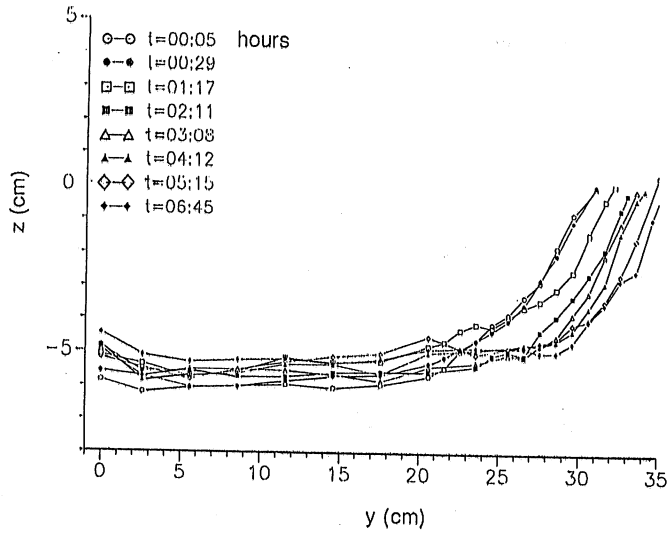

Run 8 x = 8 m

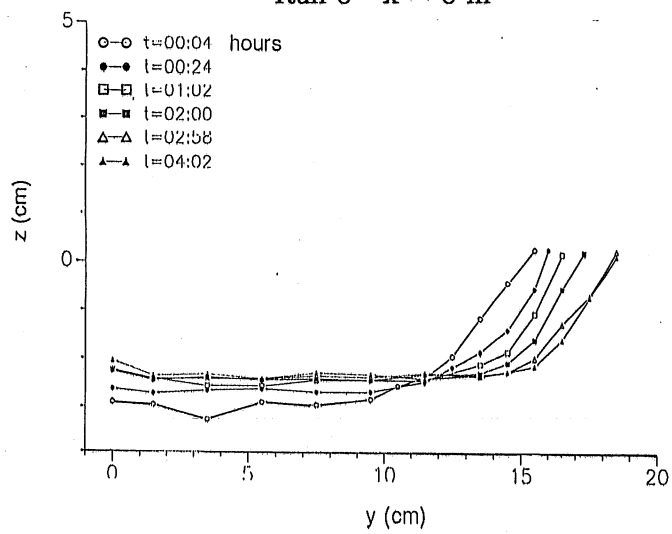

Run 11 x = 8 m

Figure 1.18. Time evolution of channel cross–sectional shape for three runs corresponding to Case 2. The profiles are of bed elevation z versus transverse position y. The times t are in hours and minutes. a) Run 4, b) Run 8, c) Run 11

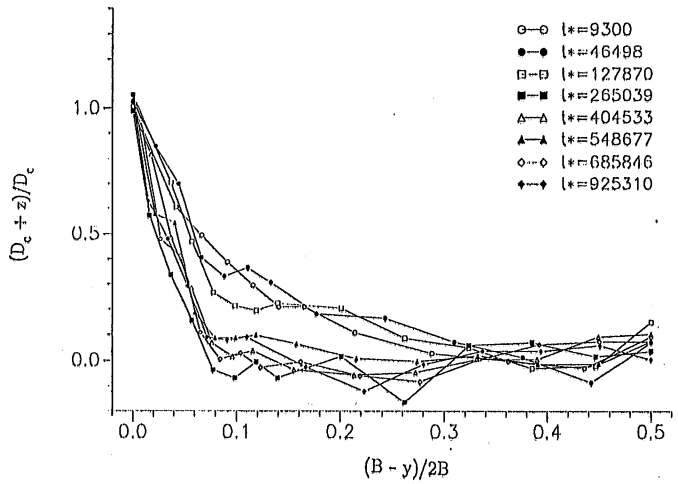

Run 4 x = 8 m

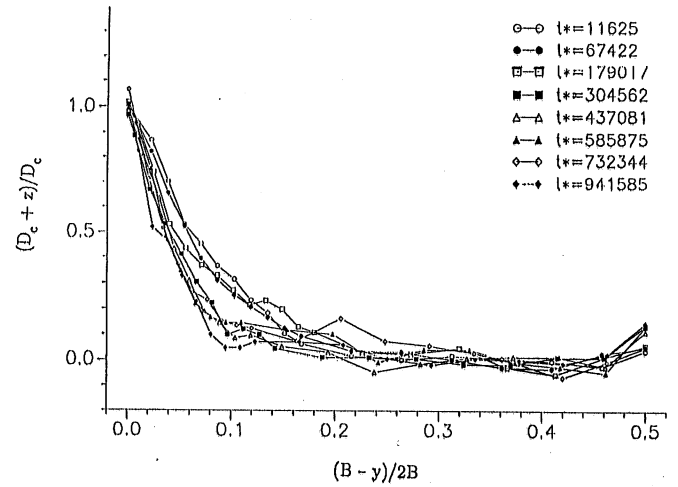

Run 8 x = 8 m

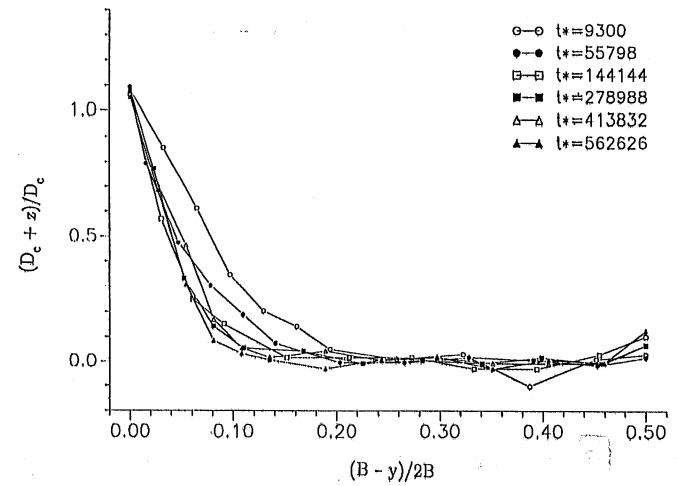

Run 11 x = 11 m

Figure 1.19 Dimensionless plots of channel cross–sectional shape at various times for three runs corresponding to Case 2. a) Run 4,b) Run 8, c) Run 11

Figure 1.20 Photo showing the definitions for the streamwise distance L between the permeable dikes, and the width B_c between the tip of the dikes and the vertical steel wall immediately opposite.

Runs 14 and 27 are of some considerable interest in terms of bank protection. In both cases, the streamwise spacing of permeable dikes L was equal to 40 cm. It can be observed from the time sequence of cross–sections shown in Figures 1.21a ~ 1.21b that the presence of permeable dikes almost eliminated bank erosion.

To obtain an idea as to the effectiveness of the dikes, it is useful to compare the cross–sectional profiles of Run 14, shown in Figure 1.21a, with those of Run 8, shown in Figure 1.18b. The hydraulic conditions for Runs 8 and 14 are very similar except for the fact that permeable dikes were absent in the former case and present in the latter case. The effectiveness of the permeable dikes in preventing bank erosion should be immediately clear.

Runs 16 and 17 form another pair of runs that are similar except for the presence or absence of permeable dikes. In Run 16 the dikes are present, but with a streamwise spacing L equal to 80 cm as opposed to the value of 40 cm of Runs 14 and 27. Comparing the cross–sectional profiles of Runs 16 and 17, as shown in Figures 1.22a and 1.22b, it is seen that the permeable dikes are not very effective in halting bank erosion. It is thus shown that the spacing of the permeable dikes must be sufficiently close in order to effect significant bank protection.

The reason that the permeable dikes afford bank protection is illustrated in Figure 1.23. This figure provides a plot of the transverse distribution of depth–averaged streamwise velocity at the end of Run 14. The extra drag of the permeable dike field in the zone $y > 22$ cm causes a marked reduction in flow velocity. This in turn reduces bed and bank shear stress, lowering the erosive potential of the flow along the erodible bank. The net result is a channel that is narrower and steeper than it would be in the absence of dikes.

Three examples of the vertical distribution of streamwise velocity for Case 3 are presented in Figures 1.24a ~ 1.24c. The measurements pertain to Run 14, and thus correspond to the raw data used to prepare Figure 1.23. The velocity profile in Figure 1.24a was measured at $y = 5$ cm; it is typical of the center portion of the channel, outside of the dike field and not too close to the vertical steel wall. The profile could be adequately fitted to a logarithmic or parabolic law.

The permeable dike field starts at $y = 22$ cm. The profile at $y = 25$ cm shown in Figure 1.24b is nearly uniform in the vertical direction. In addition, flow velocities are much reduced compared to the center region of the channel shown in Figure 1.24a. This illustrates the effect of the permeable dikes: flow velocities are both reduced and made more uniform.

Figure 1.24c shows the vertical distribution of streamwise velocity at $y = 21$ cm, i.e. in the central region of the channel just adjacent to the tip of the permeable dikes. The flow velocity is seen to have a peak at mid–depth, probably indicating the presence of secondary flow of the second type. Such secondary flow is typically seen in the corners of non–circular conduits.

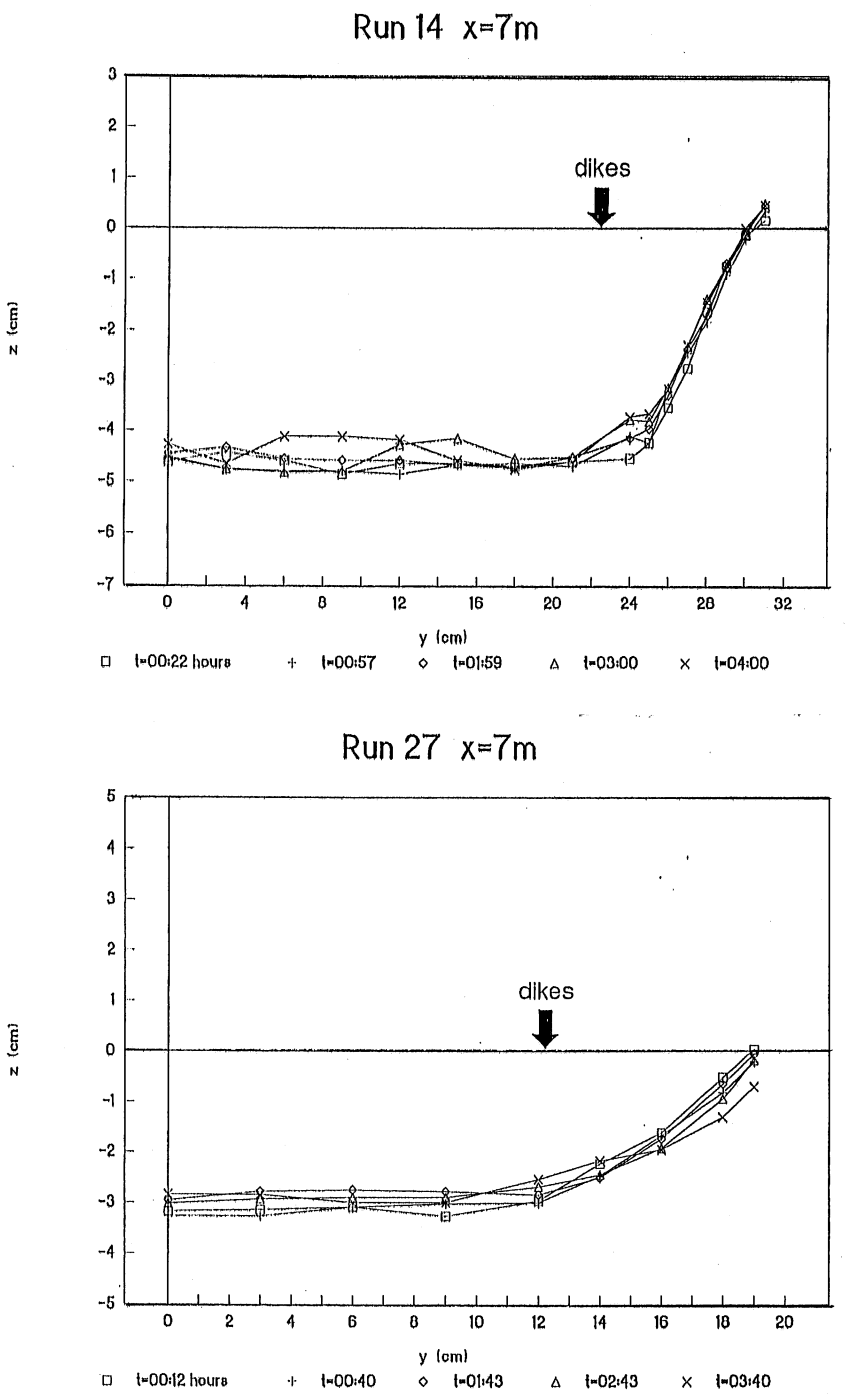

Figure 1.21 Time evolution of cross–sectional shape for two runs corresponding to Case 3. It is seen that in the presence of the permeable dikes, very little bank erosion occurs. Dike spacing L is equal to 40 cm in both runs. a) Run 14, b) Run 27, c) Run 16.

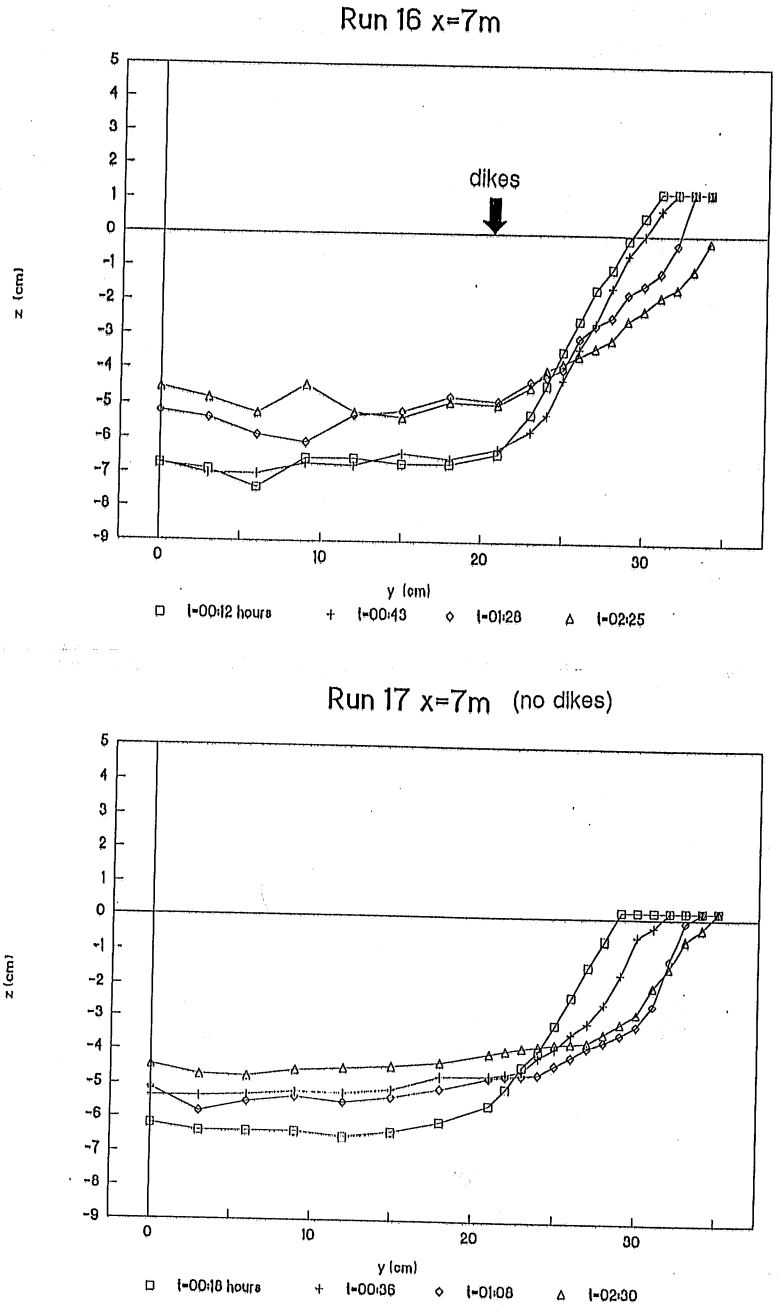

Figure 1.22 Comparison of the time evolution of cross–sectional shape for two runs, one with a dike spacing L of 80 cm and the other with no dikes. It is seen that bank erosion is not halted if L is too large. a) Run 16 (Case 3: dikes in place with L = 80 cm), b) Run 17 (Case 2: no dikes)

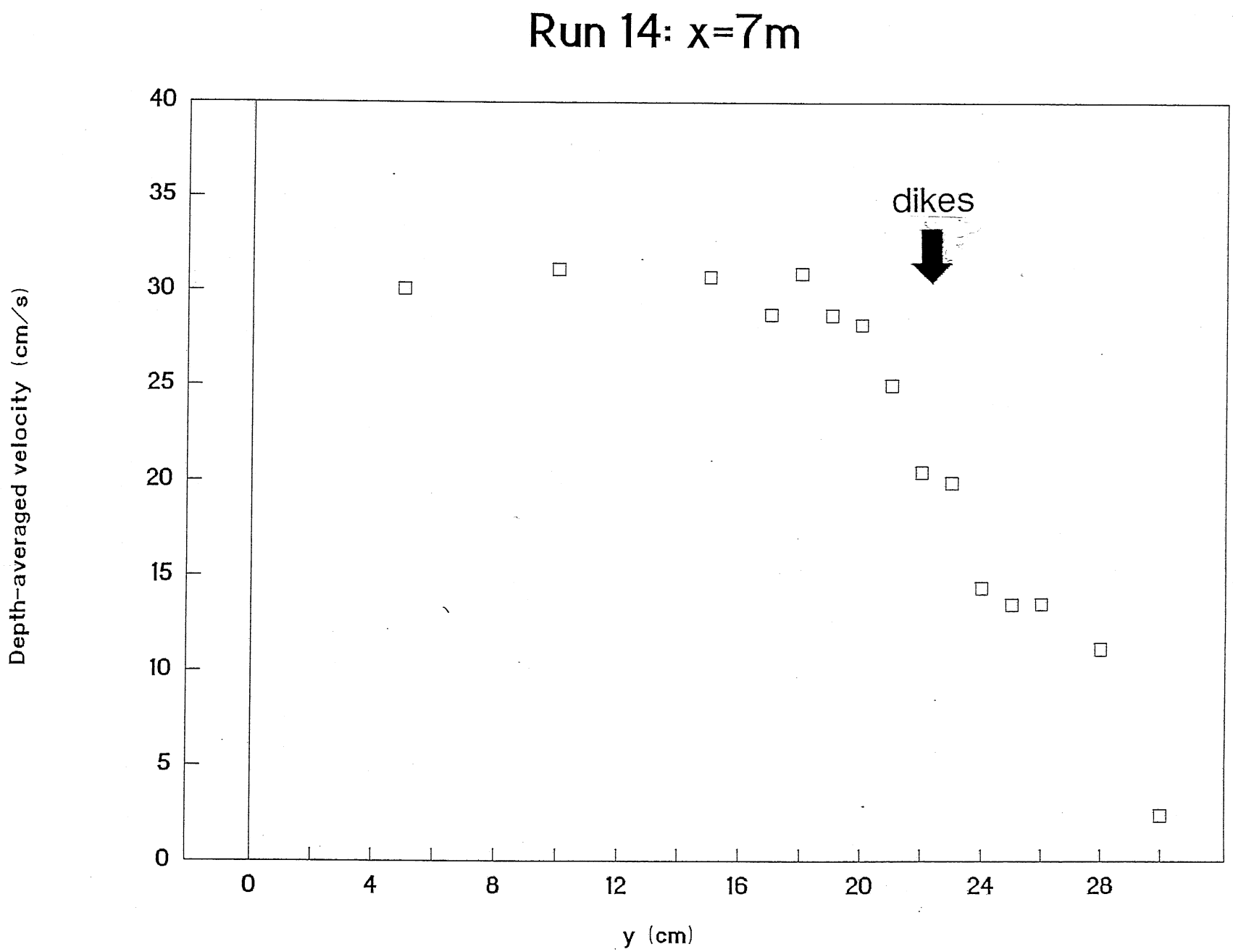

Figure 1.23 Transverse variation of depth–averaged streamwise flow velocity for Run 14, corresponding to Case 3.

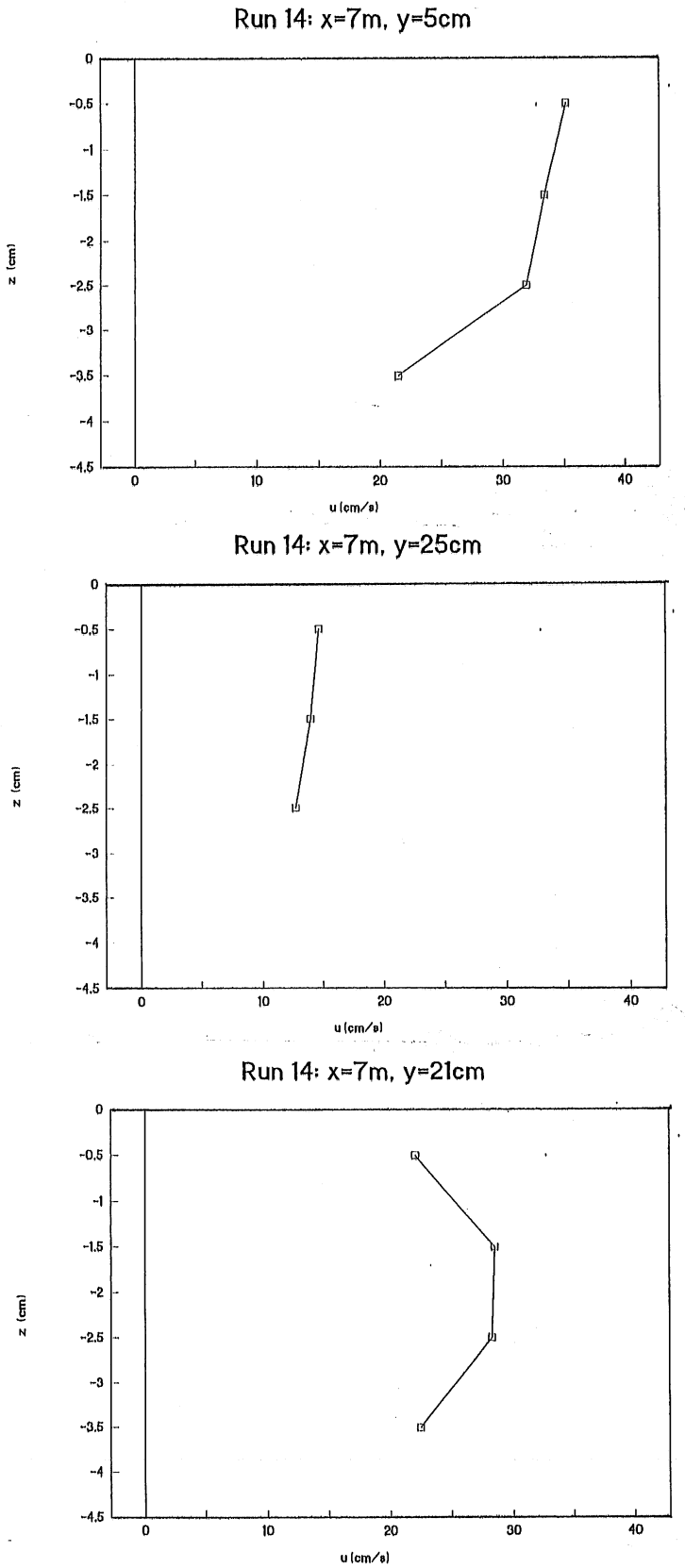

Figure 1.24 Vertical distributions of streamwise flow velocity at x = 7 m for Run 14, corresponding to Case 3. a) Distribution at y = 5 cm, corresponding to the central region of the channel, well outside of the dike field. b) Distribution at y = 25 cm, well within the permeable dike field. c) Distribution at y = 21 cm, just outside the permeable dike field.

Case 4: *Self–formed channels with suspended sediment in the absence of permeable dikes.* The set of runs corresponding to Case 4 consisted of Runs 18, 19, 20, and 28. These runs were first conducted in the absence of fines, and continued until a final near–equilibrium state had been achieved. Fines were then added to the flume, and the run continued until a new equilibrium was achieved.

It was found that two types of final equilibrium channel with fines were possible. If the supply of fines was rather low, walnut shells were left exposed on a significant portion of the bed surface. Fines accumulated in sufficient quantity to bury the walnut shells only in zones of low shear stress. An example of this case is Run 19, the bed of which is shown in Figure 1.25. Fines have accumulated substantially along the erodible bank and at the corner formed by the erodible bed and the vertical steel wall. In the center region of the channel, however, the walnut shells remain exposed.

In the case of a higher supply of fines, the bed could be completely covered by fines upon the attainment of equilibrium. An example of this is Run 28, shown in Figure 1.26. It may be said that fines are transported at capacity in Run 28, but below capacity in Run 19.

In Figure 1.27, the channel cross–section before and after the addition of fines is shown for Run 28. It is apparent that the addition of fines has totally changed the character of the channel.

Case 5: *Self–formed channels with suspended sediment and permeable dikes.* Runs 21 to 26 correspond to this case. For the purpose of comparison, Runs 22, 25, and 26 are taken as typical. The streamwise spacing L of the dikes is 40 cm for Run 22, 25 cm for Run 25, and 75 cm for Run 26. The width B_c of the center region of the channel between the tips of the dikes and the vertical steel wall was 12 cm for Runs 22 and 25 and 9 cm for Run 26.

As in Case 3, the experiments were conducted with permeable dikes in place but without fines until a near–equilibrium final state was reached. At that point fines were added, and the run continued until a new equilibrium had been obtained.

In Figures 1.28a ~ 1.28c, equilibrium cross–sectional profiles before and after the addition of fines are shown for Runs 22, 25, and 26 respectively. In all cases, substantial deposition of fines in and near the permeable dike field was achieved. This is due to the tendency for flow velocity and shear stress to be lowered within the dike field, creating a depositional environment.

Comparing these figures, it is seen that maximum deposition of fines in the dike field was realized in Run 25, corresponding to the tightest spacing of dikes (L = 25 cm). The deposit of fines grew right up to the level of the water surface. A smaller, but still substantial deposit was realized in the case of Run 22, which had a spacing L = 40 cm. In the case of Run 26, the deposit is still substantial; even though L = 75 cm, the dikes

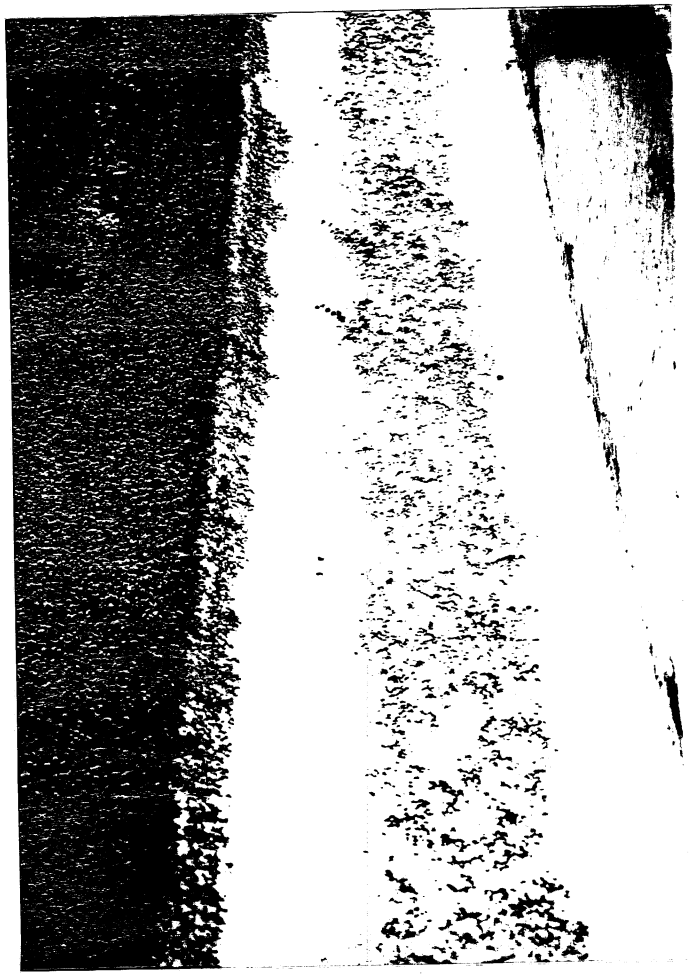

Figure 1.25 Photograph illustrating the pattern of deposition of suspended sediment for Run 19, corresponding to Case 4. The view is looking upstream. Deposition of fines is induced along the erodible bank and where the vertical steel wall meets the erodible bed, both zones of retarded shear stress. Walnut shells are still exposed in the central region of the channel.

Figure 1.26 Photograph illustrating the pattern of deposition of suspended sediment for Run 28, corresponding to Case 4. The view is looking downstream. The bed of walnut shells is almost completely buried by the deposit of fines. The supply of fines used for Run 28 was greater than that used for Run 19.

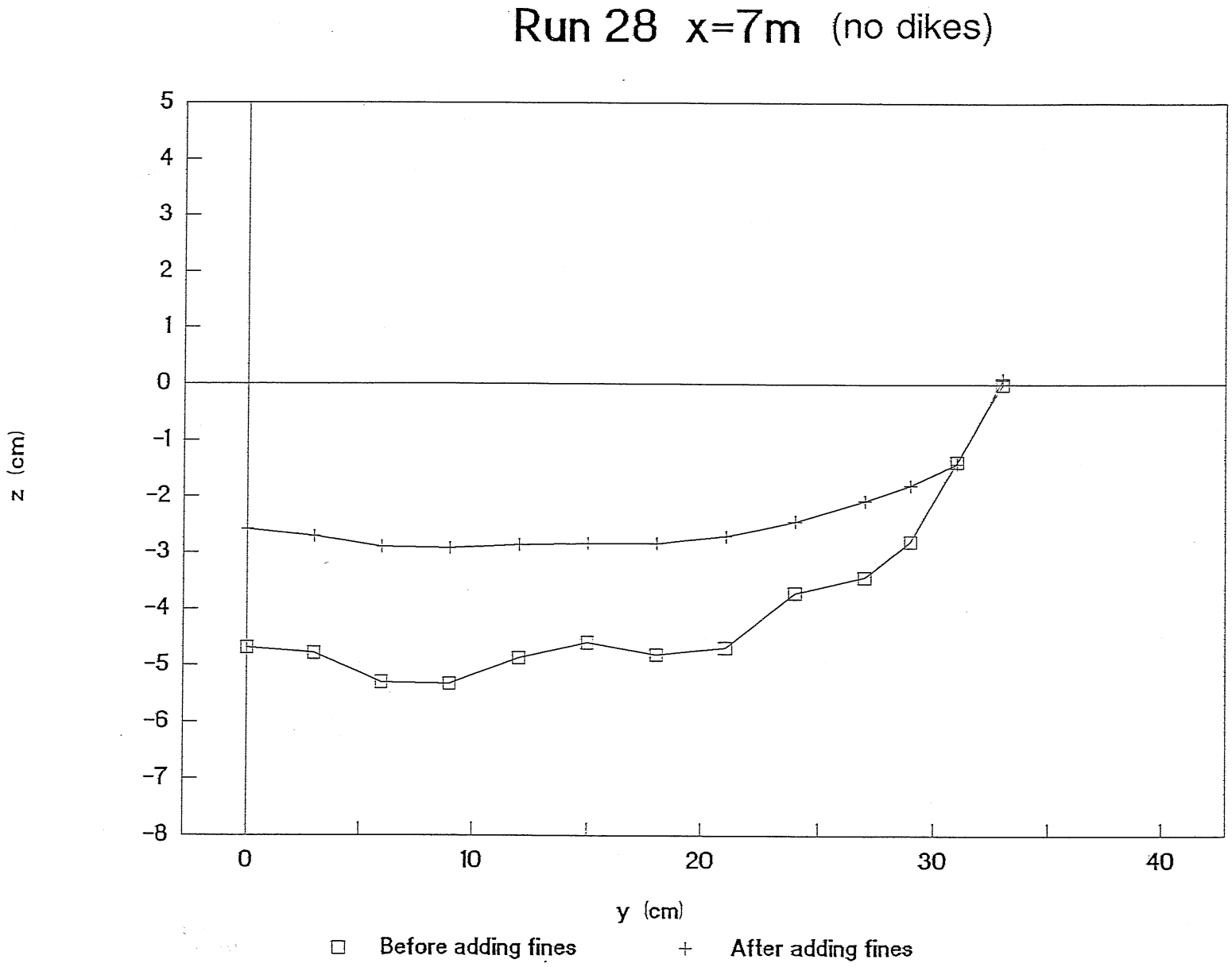

Figure 1.27 Final cross–section profiles for Run 28, before and after adding fines.

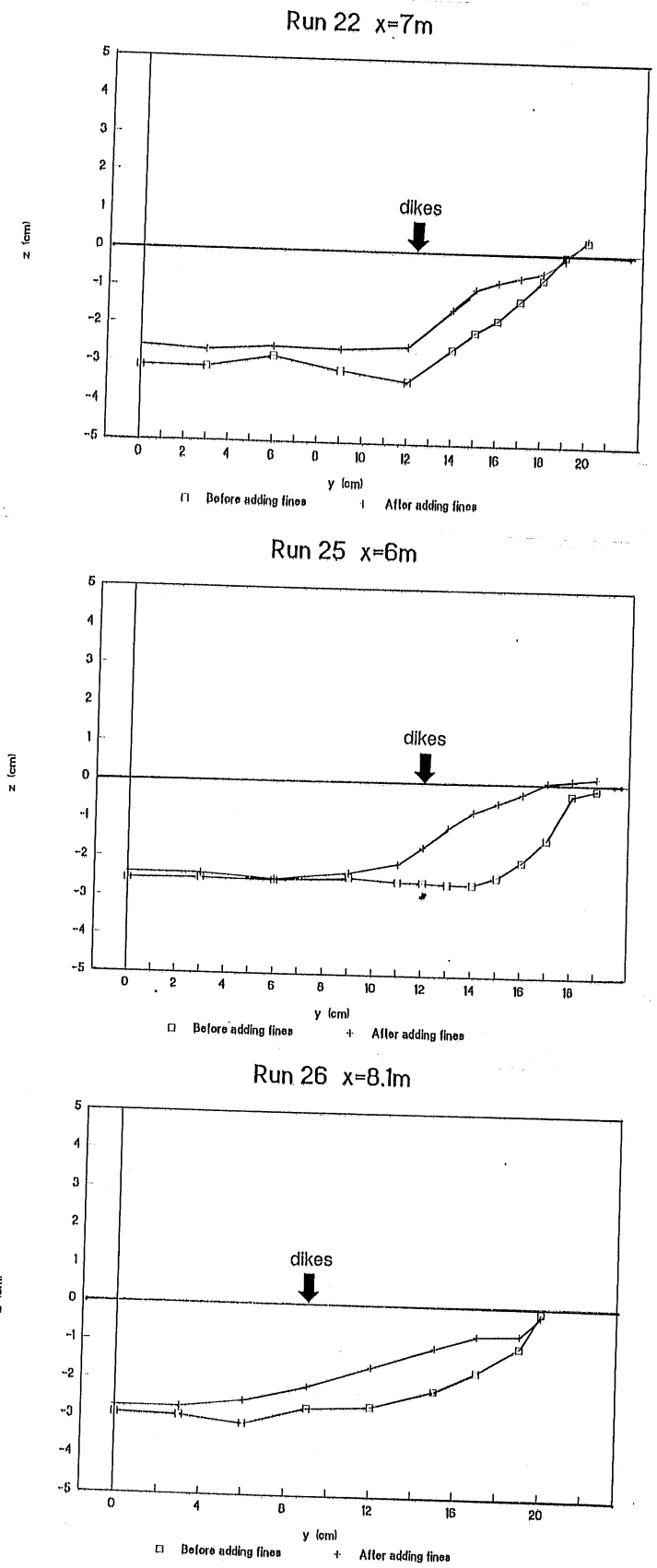

Figure 1.28 Final cross–sectional profiles for three runs corresponding to Case 5, before and after adding fines. Note the tendency for fines to accumulate within the permeable dike field. a) Run 22, b) Run 25, c) Run 26

protrude out from the bank a substantially farther distance than the other two runs. In the case of Run 26, the width of the near–bank zone protected by each dike was 11 cm (before the addition of fines); it was only 7 cm in the case of the other two runs.

The view of the channel at the end of Run 25 provided in Figure 1.29 provides visual evidence for the substantial deposit of fines that accumulated in the dike field.

In order to determine the field applicability of the experimental results on deposition of fines in permeable dike fields, it is of use to compare the cross–section of Run 25 shown in Figure 1.28b with the cross–section of the Columbia River shown in Figure 1.30 (Committee on Channel Stabilization, 1963). In both the laboratory and field case, the installation of permeable dikes is seen to have led to massive near–bank deposits. In addition, in the case of the Columbia River, the center portion of the channel deepened considerably in response to the dikes. This deepening of the central region did not occur in the laboratory experiments. This is likely due to the fact that deepening in the laboratory would have required the erosion of substantial amounts of coarse walnut shells, which are intrinsically much less mobile than the model fines. In the case of the reach of the Columbia River, the channel is composed of suspendable sand everywhere.

Figure 1.31 shows the transverse distribution of depth–averaged streamwise flow velocity for Run 22. It is seen that flow velocity is substantially reduced in the permeable dike field, in correspondence to Figure 1.23. When fines are carried in suspension, this lowering of flow velocity creates a depositional environment, allowing for the accumulation of fines in the dike field evidenced in Figures 1.28a ~ 1.28c.

1.6 DATA ANALYSIS

The data analysis performed here is not intended to be complete. It only provides a hint as to how the experimental results could be used to improve the design of low–cost bank protection works.

As pointed out earlier, the data in Table 1 pertains only to the final equilibrium without fines, whether or not fines were added later (as in Cases 4 and 5). The equilibrium channels formed in walnut shells provide accurate models of gravel–bed streams (e.g. Parker, 1978; Ikeda et al., 1988).

According to Ikeda et al. (1988), the stable center depth of straight gravel river without fines (and in the absence of permeable dikes) can be calculated using the following equation:

Figure 1.29 Photograph illustrating the final state attained in Run 25 after the addition of fines. The view is looking downstream. Note that the walnut shells are exposed in the central region of the channel, but a thick deposit of fines has accumulated in the dike field.

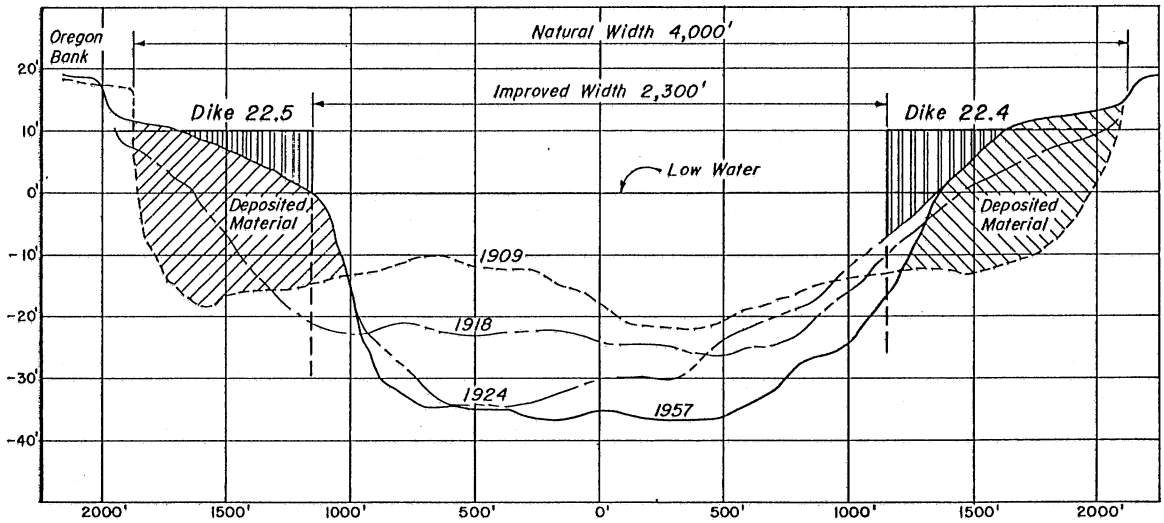

COLUMBIA RIVER AT HENRICI BAR - MILE 91

NOTE:
Dike 22.4, 840' long, built 1918, extended 300' in 1932
Dike 22.5, 900' long, built 1918

Figure 1.30 Diagram illustrating the change in channel cross-section on the Columbia River at Henrici Bar (mile 91) resulting from the installation of permeable dikes.

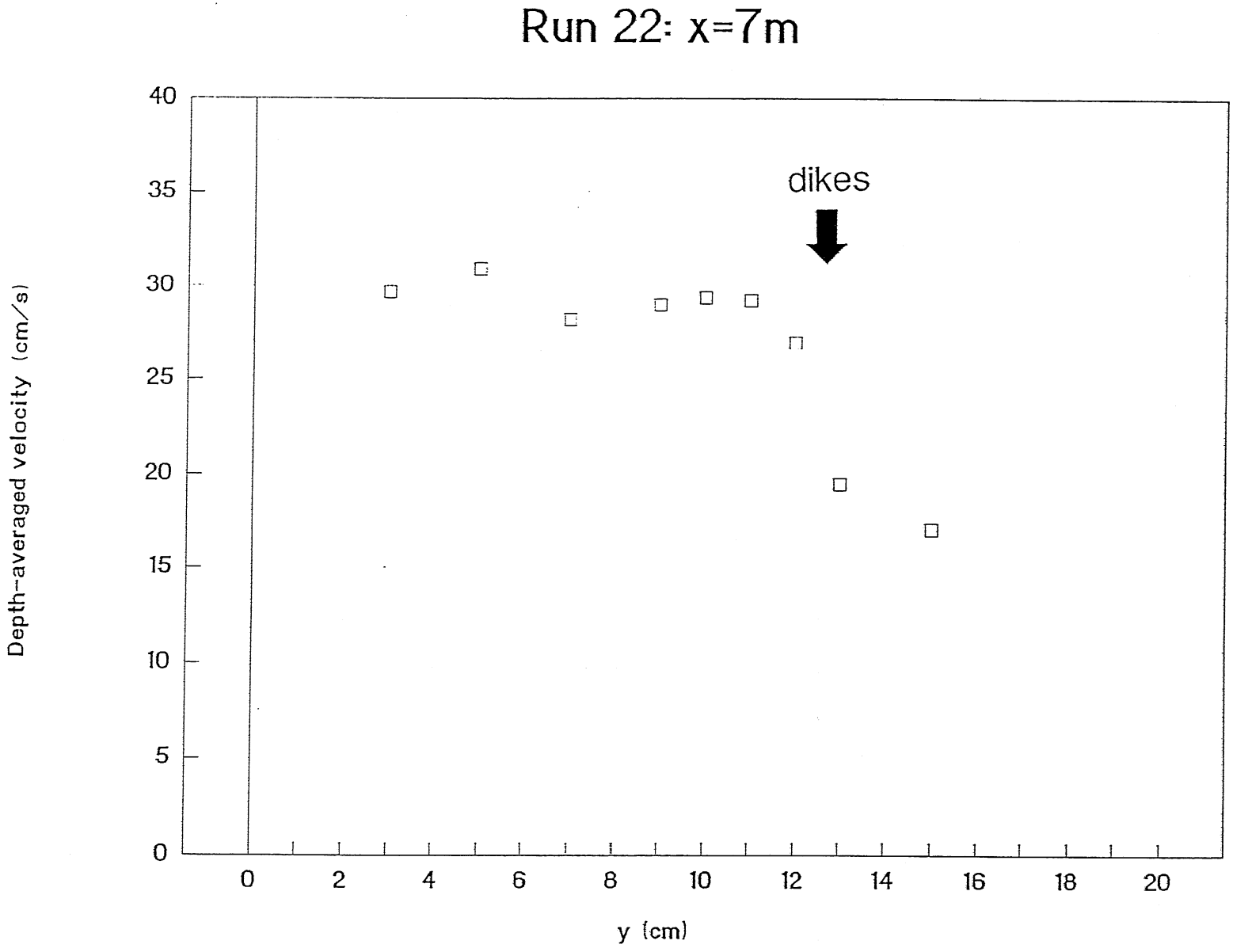

Figure 1.31 Transverse variation of depth–averaged streamwise flow velocity for Run 22, corresponding to Case 5.

$$D_c = 1.23 \cdot \frac{0.05}{\left[\log_{10}(19\frac{d_{c50}}{d_{c90}})\right]} R\sigma d_{c50} S^{-1} \qquad (1\text{–}7)$$

Here $\sigma = d_{c90}/d_{c50}$.

In deriving the above equation, the critical Shields stress τ^*_{cr} was set equal to 0.0306 for uniform sediment. The results of the experiments of case 1, however, indicate that a more appropriate value for the case of walnut shells is 0.04. Using this modified value, (1–7) can be amended to

$$D_c = 0.0492\ R d_{c50} S^{-1} \qquad (1\text{–}8)$$

In the case of the present experiments, R is equal to 0.41, σ equal to 1.13, and D_{c50} equal to 2.6 mm. The above relation can thus be reduced to

$$D_c = 0.0052\ S^{-1} \qquad (1\text{–}9)$$

The above equation thus defines a predictive relation for stable center depth in the absence of fines.

Ikeda et al. (1988) found the following relation for stable channel width in the absence of fines (and the absence of permeable dikes as well):

$$B = \frac{Q}{D_c(gD_cS)^{1/2} \cdot 5.76 \cdot \log_{10}(7.333\ \frac{D_c}{\sigma d_{c50}})} + 0.5 \cdot \left[2.571 + \frac{0.8972}{\log_{10}(7.333\ \frac{D_c}{d_{c50}})}\right] D_c \qquad (1\text{–}10)$$

The data for D_c and B from Table 1, which pertain to near–equilibrium channels without fines (or before fines were introduced) of Table 1, were used to test the above relations. The results are shown in Figures 1.32a and 1.32b. It is seen that the theory predicts the data quite well when permeable dikes are not present. On the other hand, the channels for which permeable dikes were present show a much larger depth and smaller width than that predicted by the theory of Ikeda et al. (1988). One may conclude that the effect of the permeable dikes is to increase depth and reduce width compared to the equilibrium case in their absence. This observation forms the basis for a measure of the effectiveness of permeable dikes in preventing bank erosion.

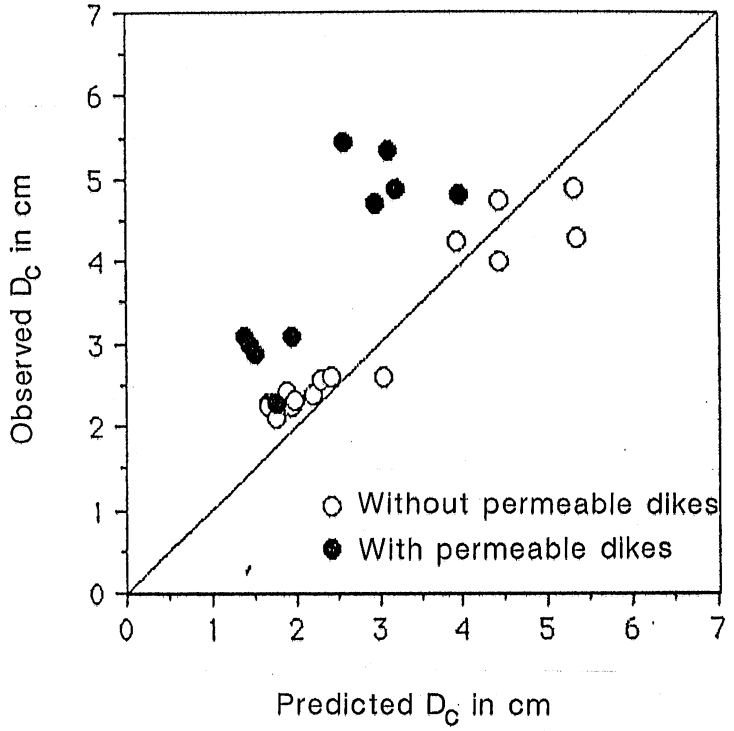

Figure 1.32 a) Test of predicted versus observed final center depth D_c for the laboratory data. The effect of dikes has been neglected.

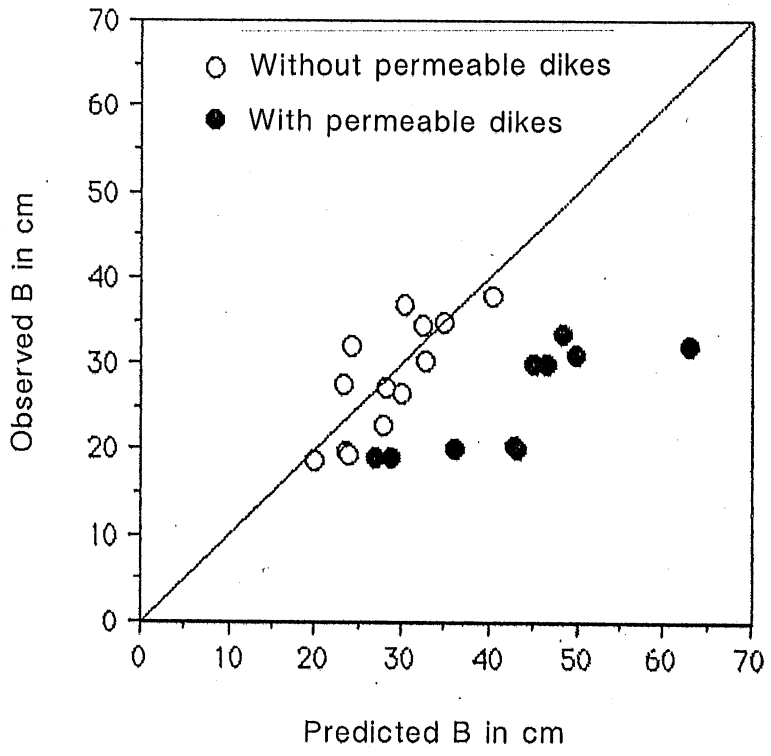

Figure 1.32 b) Test of predicted versus observed final water surface width B for the laboratory data. The effect of dikes has been neglected.

As noted earlier, permeable dikes constitute a special case of distributed drag. Recently Ikeda and Izumi (1990) have developed a theory for equilibrium channel depth and width in the presence of distributed drag. The theory was developed for the case of near–bank vegetation, but it generalizes in a natural way to the case of permeable dikes.

The complete theory of Ikeda and Izumi (1990) is not reviewed here. It is simply pointed out that the dimensionless parameter in the theory controlling the effect of distributed drag is χ, where

$$\chi = \frac{C_D d_p D_c}{2 \ell_x \ell_y C_f} \tag{1–11}$$

Here C_D denotes the drag coefficient for a cylinder, under the assumption that the permeable dikes are constructed from cylindrical members, C_f denotes the bed friction coefficient of the flow in the absence of permeable dikes, given by

$$C_f = \frac{\tau_b}{\rho U^2} \tag{1–12}$$

where τ_b denotes bed shear stress and U denotes cross–sectionally averaged flow velocity, d_p denotes the diameter of the cylindrical members (piles) composing the dikes, and ℓ_x and ℓ_y denote the longitudinal and transverse distance between members.

For the purposes of the present studies a value of C_D of 1.5 was adopted (Li and Shen, 1982; Ikeda et al., 1991). Computed values of the dimensionless measure of dike effectiveness χ and bed friction coefficient C_f are listed in Table 2 for all runs in which permeable dikes were employed.

With this in mind, the data of Table 1 are re–analyzed, such that observed values of D_c and B are compared against values computed from (1–9) and (1–10) in the absence of permeable dikes, and the theory of Ikeda and Izumi (1990) in their presence. The results are shown in Figure 1.33a and 1.33b. The predicted values are seen to correspond quite well to the data.

It is thus seen that the relations of Ikeda and Izumi (1990) constitute a good design basis for the design of permeable dikes, and by extension, any bank protection technique involving distributed drag, including the Palmiter method. These relations do not, however, include the added benefit resulting from the deposition of fines in the zone of retarded flow.

Table 2. Summary of permeable dike parameters

Run No.	a, m^{-1}	C_f	χ
14	0.0159	0.00879	1.32
15	0.0318	0.0107	2.79
16	0.0177	0.0394	1.47
21	0.0201	0.0104	1.33
22	0.0202	0.0222	1.34
23	0.0349	0.00929	3.03
24	0.0306	0.00810	2.50
25	0.0239	0.00625	1.35
26	0.0101	0.0127	0.643
27	0.0195	0.0147	1.27

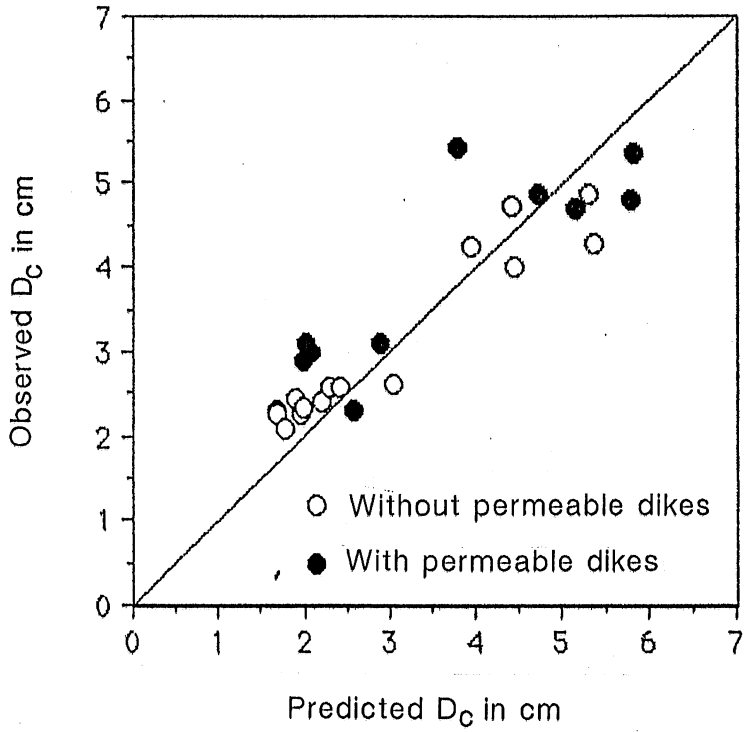

Figure 1.33 a) Test of predicted versus observed final center depth D_c for the laboratory data. The effect of dikes has been included.

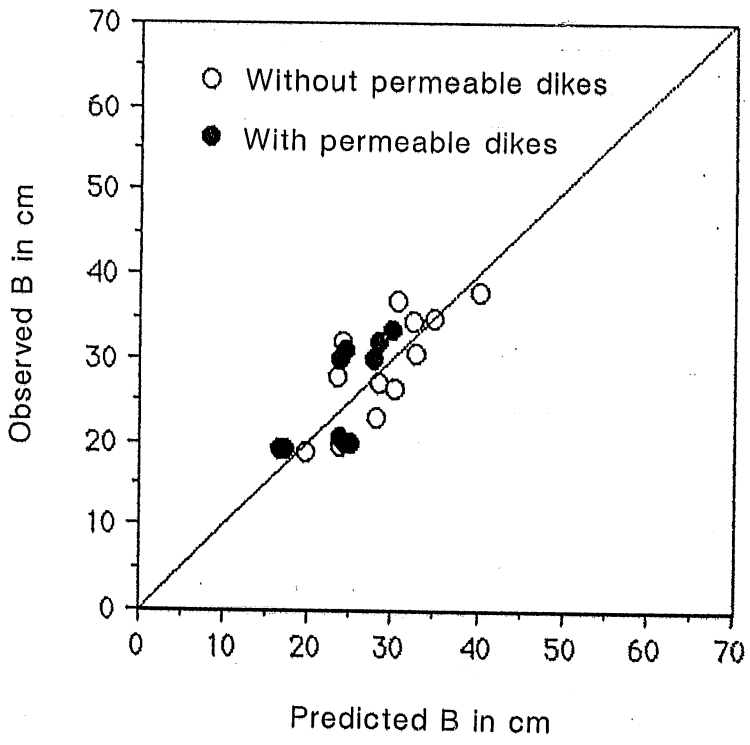

Figure 1.33 b) Test of predicted versus observed final water surface width B for the laboratory data. The effect of dikes has been included.

1.7 CONCLUSIONS

The experiments reveal that it is possible to model processes involving both coarse–bedded and fine–bedded self–formed streams at reduced scale in the laboratory. Coarse–bedded streams were modeled with lightweight walnut shells with a median diameter of about 2.6 mm. This material moved essentially as bedload. Fines were modeled using 0.12 mm lightweight plastic particles (vinyl chloride homo–polymer). These particles could move as bedload, but were also easily suspended.

It was demonstrated that not only the final equilibrium state, but the processes of bank erosion and deposition leading to that final state could be modeled successfully in the laboratory. The study was restricted, however, to straight channels.

The placement of distributed drag such as permeable dikes, jacks, and trees placed according to the Palmiter method can allow for a considerable degree of bank protection. The experiments indicate that the bank protection derives from two different sources.

The first of these is the direct action of the distributed drag to retard near–bank flow velocities. This in turn reduces the shear stress on the bank, and thus the potential for bank erosion. The experiments demonstrate that distributed drag can provide effective bank protection regardless of whether the eroding bank is composed of coarse–grained or fine–grained material.

If the river also contains a substantial load of fine–grained material carried in suspension, this material is available for deposition in the zone of low velocity created by the distributed drag field. In this way not only can bank erosion be halted, but a previously–eroded bank can be induced to build back.

The degree of bank protection provided is proportional to the density of the units of distributed drag placed along the banks. In the case of the Palmiter method, these units are felled trees.

Appropriate design techniques for bank protection using distributed drag can be obtained by an application of the theory of Ikeda and Izumi (1990). This theory does not include the effect of suspended sediment. Such a theory is presently being formulated.

1.8 REFERENCES

Andrews, E. D. 1984 Bed–material entrainment and hydraulic geometry of gravel–bed rivers in Colorado, *Geol. Soc. Am. Bull.* 95, 371–378.

Bentley, C., Parker, G., & Leuthe, D. 1991 Streambank erosion: gaining a better understanding. Brochure, Division of Water Resources, Minnesota Department of Natural Resources, St. Paul, Minnesota.

Charlton, F. G., Brown, F. M. & Benson, R. W. 1978 The hydraulic geometry of some gravel rivers in Britain, 48 pp., Hydraul. Res. Stn, Wallingford, Great Britain.

Committee on Channel Stabilization 1963 Symposium on channel stabilization problems. Technical Report No. 1, Vol. 1, U. S. Army Corps of Engineers, Vicksburg, Mississippi.

Glover, R. E. & Florey, Q. L. 1951 Stable channel profiles. U. S. Bureau of Reclamation, Hydr. No. 325.

Hirano, M. 1973 River bed variation with bank erosion. *Proc. Japan Soc. Civil Engrs*, No. 210, 13–20 (in Japanese).

Ikeda, S. 1981 Self–formed straight channels in sandy beds. *Proc. ASCE., J. Hydraul. Div.*, 107(HY4), 389–406.

Ikeda, S. & Izumi, N. 1990 Width and depth of self–formed straight gravel rivers with bank vegetation. *Water Resources Research*, 10, 2353–2364.

Ikeda, S., Izumi, N. & Itoh, R. 1991 Effects of pile–dikes on flow retardation and sediment transport. *J. Hydraul. Eng.* (in press).

Ikeda, S., Parker, G. & Kimura, Y. 1988 Stable width and depth of straight gravel rivers with heterogeneous bed materials. *Water Resources Research*, 24, 713–722.

Lane, E. W., Lin, P. N. & Liu, H. K. 1959 The most efficient stable channel for completely clean water in non–cohesive material. Colorado State Univ., Rep. CER 59 HKL 5.

Leopold, L. B. & Maddock, T. Jr. 1953 The hydraulic geometry of stream channels and physiographic implications. U. S. Geol. Surv. Prof. Paper No. 252.

Li, R. M. & Shen, H. S. 1973 Effect of tall vegetations on flow and sediment. *Proc. ASCE, J. Hydraul. Div.*, 99(HY5), 793–814.

MacDonald, T., Parker, G., & Leuthe, D. 1991 Comprehensive inventory and analysis of river meander problems in Minnesota. Project Report No. 321, St. Anthony Falls Hydraulic Laboratory, University of Minnesota, Minneapolis, Minnesota.

Parker, G. 1978a Self–formed straight rivers with equilibrium banks and mobile bed. Part 1. The sand–silt river. *J. Fluid Mech.*, 89, 109–125.

Parker, G. 1978b Self–formed straight rivers with equilibrium banks and mobile bed. Part 2. The gravel river. *J. Fluid Mech.*, 89, 127–147.

Parker, G. 1982 Stability of the channel of the Minnesota River near State Bridge No. 93, Minnesota. Project Report No. 205, St. Anthony Falls Hydraulic Laboratory, University of Minnesota, Minneapolis, Minnesota.

Wolman, M. G., and Brush, L. M. 1961 Factors controlling the size and shape of stream channels in coarse non–cohesive sands. U.S. Geol. Survey Prof. Paper No. 282–G.

PART 2 THEORETICAL STUDY OF BANK EROSION AND RESULTANT EVOLUTION OF STRAIGHT CHANNELS

2.1 INTRODUCTION

Until recently, it has not been possible to predict river bank erosion in a quantitative way. As a result, most methods of bank protection are based on experience. In the research presented here, an attempt is made to predict bank erosion in a detailed way in the context of a straight river channel. The research described here is essentially theoretical and computational in nature. It is intended to complement the experimental program described earlier.

A straight channel with an initially narrow, trapezoidal cross–section in non–cohesive material is considered. The channel banks are allowed to erode, so that in time the channel approaches a stable cross–sectional shape.

The goal of the research, then, is to produce a physical model and a computer program which can simulate the time evolution of the cross–section of a straight river channel from an initial cross–sectional shape. This includes the modeling of both the flow field and the transport of sediment.

The sediment can be transported in two ways: as suspended load and/or as bedload. In the case of suspended load the particles are carried by the turbulence of the fluid and are essentially out of contact with the bed. In the case of bedload transport the particles move on the surface of the bed via sliding, rolling and saltating. In most cases of interest, saltation tends to be the dominant mode.

The version of the numerical model prepared for this study incorporates only bedload transport. The details of the research described below serve to quantify the interaction of the bed and the flow field through bedload transport. As a result of this interaction the initial cross–sectional shape of the channel metamorphoses until a dynamic equilibrium is reached. At this dynamic equilibrium the cross–sectional shape does not change in time. The river carries sediment in the middle, flat portion of the channel, while the bedload transport is vanishing on the banks. Until this equilibrium state is reached the bank erodes and the sediment deposits in the middle of the channel. Practically, this means that the river tends to become wider and shallower.

This description grasps the essential features of bank erosion in natural rivers. Knowing the discharge, the slope of the bed, and the size and density of the bed material, it is possible to predict the evolution of cross–sectional shape in straight river channels dominated by bedload transport.

In many cases bank erosion is undesirable. In future research the effect of permeable dikes, the Palmiter method, and other means of distributed drag as means of bank protection will be investigated. In addition, suspended sediment will be included into the model.

As an example, a permeable dike field is shown in Figure 1.12. The effect of permeable dikes in the absence of suspended sediment is to slow the flow down near the banks. This reduces the shear stress acting on the banks, thus stopping or mitigating bank erosion. At the same time, the flow velocity is increased in the middle portion of the channel. In the presence of suspended sediment, the permeable dikes not only stop the erosion of the banks, but can also act to build the banks back. As the flow has been been slowed down within the dike field, the flow cannot support as much suspended sediment load as it might otherwise, so the sediment deposits in this area. The modeling of the suspended sediment and the permeable dikes as distributed resistance will complete the program.

In the succeeding sections, the part of the numerical model completed to date will be described, and the results will be demonstrated.

2.2 NUMERICAL MODELING OF THE FLOW FIELD

Consider a straight river channel in which the flow is one–dimensional and has a velocity component only in the streamwise direction. Straight–channel secondary currents are neglected as insignificant in this case. The distribution of the streamwise velocity over the cross–section is important for two reasons. The first reason is that it makes possible the calculation of the water discharge at any time. The second reason is that the local shear stress distribution on the bed can be derived from it as well.

The governing equation of the flow field, that is, the so called Navier–Stokes equation, can be solved only numerically if the geometry of the flow is of the natural shape. As the flow considered is turbulent, the streamwise Reynolds equation is derived from the streamwise Navier–Stokes equation. To calculate the turbulent eddy viscosity in the flow a simple turbulent closure model is introduced. The significance of solving this partial differential equation with a turbulent closure model is that a reasonably accurate shear stress distribution on the bed can be obtained.

The present formulation includes the phenomenon of lateral bankward transport of streamwise fluid momentum due to turbulence. Previous models not calculating this feature failed to find any dynamic equilibrium shape of the cross–section. The turbulence in the flow tends to carry momentum from the center of the channel towards the banks.

As a result of this momentum transport the velocity increases somewhat near the banks, with a concomitant decrease in the middle of the cross–section. This velocity distribution results in a realistic distribution of shear stress on the bed.

The time scale of change in the flow field is much smaller than the time scale of change in channel shape due to bedload transport. In other words the flow adjusts to the changes in cross–sectional shape almost immediately. As a result, the time derivative in the Reynolds equation can be neglected. The partial differential equation so obtained describes a quasi–steady flow field.

To solve this differential equation on the domain corresponding to the cross–section of the flow, appropriate boundary conditions must be prescribed. On the bed, the so called slip boundary condition is specified. A thin inner layer is attached to the flow field. In this inner layer, it is assumed that the velocity can be calculated from the logarithmic law of the wall for fully rough flow. On the water surface vanishing shear stress is prescribed.

The streamwise quasi–steady Reynolds equation with the above boundary conditions are solved with the Finite Element Method. Using the Finite Element Method the flow field is discretised into small triangular elements. Over each and every element the velocity field is approximated with bilinear basis functions which span a small plane velocity surface over the elements. This spatial discretization results in an algebraic system of equations which is solved with Gaussian elimination.

The calculation is an iterative process, according to which convergence is measured with the root mean square error in the shear stress distribution. The advantage of the application of the Finite Element Method for this problem is that the geometry of the flow field can easily be approximated.

It should be emphasized again that the essential feature of the numerical modeling of the flow is that an inhomogeneous nonlinear partial differential equation of fluid mechanics has to be solved on an unusual domain to obtain the correct velocity and shear stress distribution.

The partial differential equation of the flow field is:

$$\frac{\partial}{\partial y}\left[(\mu + \mu_t)\frac{\partial u}{\partial y}\right] + \frac{\partial}{\partial z}\left[(\mu + \mu_t)\frac{\partial u}{\partial z}\right] + \rho g S = 0 \qquad (2\text{–}1)$$

Here,

u = u(y,z) is the streamwise velocity,
x,y,z = streamwise, lateral, vertical coordinates,
ρ = water density,
g = gravitational acceleration,
S = streamwise slope of the channel,
μ = molecular viscosity of water,
μ_t = turbulent eddy viscosity of the flow.

The eddy diffusivity is μ_t is given by the following relation:

$$\mu_t = \sqrt{\tau_o/\rho}\ \kappa\ n\ (1 - \frac{n}{D_n}) \qquad (2\text{–}2)$$

where,

τ_o = bed shear stress,
κ = the von Karman constant, taking a value of 0.40,
n = local coordinate upward normal to the bed, and
D_n = depth measured upward normal from the bed.

The boundary condition on the bed is:

$$u_{bed} = \frac{1}{\kappa}\sqrt{\tau_o/\rho}\ \ell n(\frac{n_{match}}{k_s}\ 30) \qquad (2\text{–}3)$$

where

n_{match} = thickness of the inner matching layer,
$k_s = 2.5\ d_{50}$ = the roughness height, and
d_{50} = median grain diameter of the sediment.

The bed shear stress is obtained from the velocity distribution as follows:

$$\tau_o = (\ \mu + \mu_t\ )\ \frac{\partial u}{\partial n}\Big|_{bed} \qquad (2\text{–}4)$$

The cross–section is assumed to be symmetric so that the differential equation is solved on the half domain shown in Figure 2.1, in which the cross–section and the coordinate system are illustrated.

2.3 MODELING OF EROSION AND DEPOSITION IN THE CROSS–SECTION: THE SEDIMENT TRANSPORT MODEL

The evolution of cross–sectional shape in time is described by the sediment continuity or Exner equation. This is a partial differential equation in which the bed elevation is function of time and space. The one–dimensional Exner equation for the present problem is;

$$\frac{\partial z}{\partial t} + \frac{1}{1-\lambda_p}\frac{\partial}{\partial y}\ q_y = 0 \qquad (2\text{–}5)$$

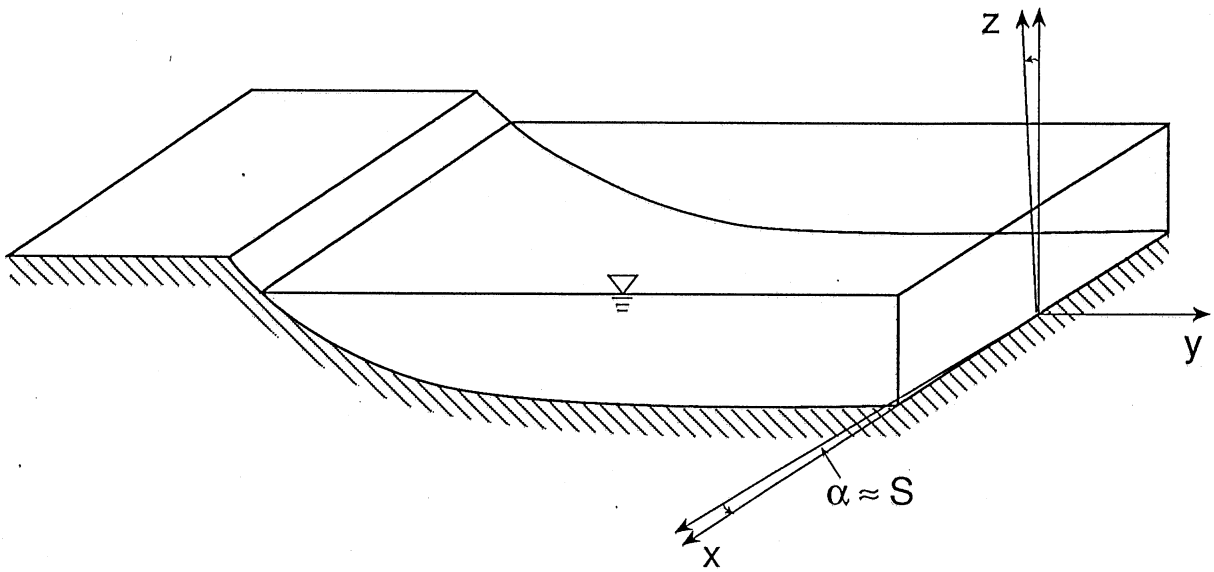

Figure 2.1. The half channel cross–section and the coordinate system.

where

z = bed elevation,
λ_p = porosity of the sediment,
t = time, and
q_y = volume bedload transport rate per unit width in the y–direction.

To solve this equation it is necessary to have a predictive relation for transverse bedload transport rate q_y. In the literature, there are many formulations developed to predict transverse bedload transport. Some of them were tried during the development of the numerical model, but they did not perform well. So far these formulations were derived for special cases for which the inclination of the bed both in lateral (y) and streamwise (x) directions are small. In the present case, at the edge of the water surface the angle of the bank inclination is high, close to the angle of repose, as it can be seen on Figure 2.2. When such conditions prevail, existing relations are found to break down. This is particularly true because an erosional front tends to develop in the present case, working its way up the bank as it is illustrated in Figure 2.3.

The initiation of movement of sediment and the quantity of the sediment which is in motion depends on the magnitude of the shear stress exerted by the flow field on the bed. It is thus important to have an accurate shear stress distribution on the bed. Knowing the shear stress distribution and the critical shear stress at each point on the bed, the position of the erosional front can be determined. Where the shear stress is higher then the critical shear stress the sediment is in motion; where it is lower there is no sediment moving. These two regions are separated by the front of erosion as shown in Figure 2.4.

The sediment flux vector is calculated from the shear stress in the region where the sediment is in motion. Thus, it is obtained from the critical shear stress, the shear stress, the angle of the bed inclination in the streamwise and lateral directions, and other parameters characterizing the sediment on the bed. Due to the failure of previous bedload formulations a new bedload relation had to be derived and tested.

This new relation is described in more detail in Kovacs and Parker (1991a). The new relation is nonlinear, fully vectorial, and based on a generalization of the Bagnold hypothesis (1956). The mean velocity vector of the sediment motion is obtained from the force balance on a sediment particle placed on a surface which is tilted in two (streamwise and lateral) directions. The force balance equation is not simplified assuming small angles. Because of its fully nonlinear nature as regards bed slope, this formulation can be used for high angles, i.e. up to near the angle of repose.

Thus far the Bagnold hypothesis, used to calculate the sediment content of the bedload layer, has been applied only to one–dimensional problems, i.e unidirectional streamwise transport of bedload over horizontal beds. In the present case the bedload transport must be two–dimensional

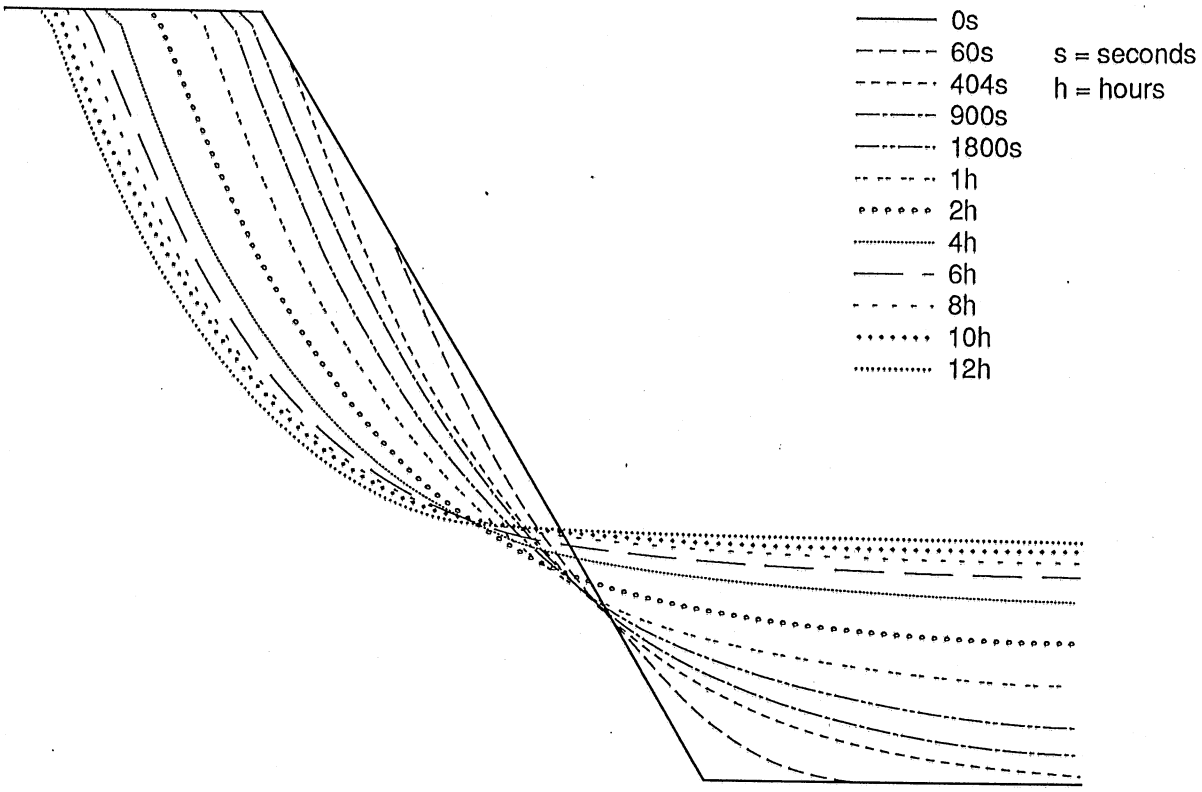

Figure 2.2. Time evolution of the cross–section.

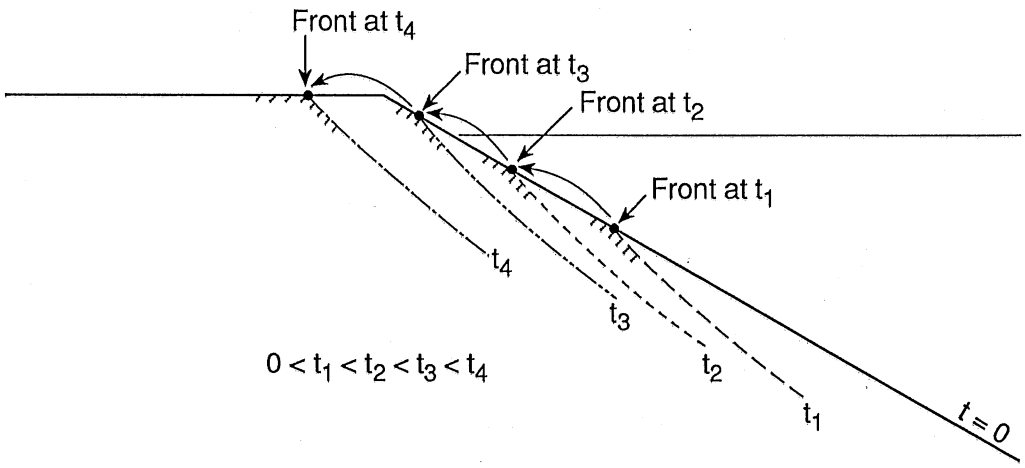

Figure 2.3. Migration of the front.

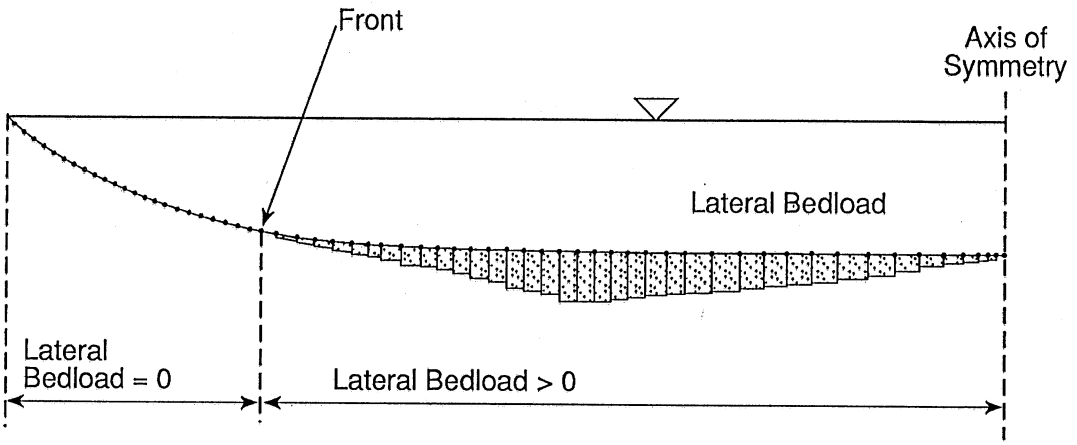

Figure 2.4. Definition of the front of erosion.

because the sediment moves both in the streamwise and the lateral directions. This is illustrated in Figure 2.5. A major consequence of this feature is that the Bagnold hypothesis must be generalized so as to handle the fully vectorial case.

To solve the Exner equation, appropriate initial and boundary conditions must be prescribed. The initial condition is the geometry of the cross–section is given at the beginning, i.e. at time $t = 0$. This initial shape was chosen to be trapezoidal, as this shape is convenient to reproduce in the laboratory. The boundary condition is prescribed at the front of erosion, where the bed elevation is still equal to its initial value (see Figures 2.3 and 2.4).

In the numerical solution, the space discretization is done with the Finite Element Method, while the integration in time is carried out with the variable–step trapezoid rule. The advantages of the Finite Element Method are that it can be fitted to the space discretization of the flow field, and that the migration of the erosion front can be traced. The variable–step trapezoid rule provides a scheme which can follow the change in the time scale of the sediment transport phenomena. When the process slows it automatically chooses a larger time step, making the computation more cost–effective by reducing the total computational run time.

The numerical modeling of the sediment transport in the cross–section can be summarized as follows. A new bedload formulation has been developed and tested. The numerical solution of both the flow field and the bed solution appear to provide reasonable results, as will be demonstrated in the next section.

A complete summary of both the nonlinear bedload model and the calculation of channel evolution can be found in Kovacs and Parker (1991a,b).

2.4 EXAMPLE CALCULATION: COMPARISON WITH DATA

To demonstrate the capability of the above–described numerical model, the predictions yielded by it are compared against data from the literature. The case chosen for comparison is Run 17 of Ikeda (1981).

Run 17 of Ikeda (1981) provides a representative case of an experiment on river widening in which an initially trapezoidal section is provided. It is of particular interest in that fairly complete data are available for the time evolution of the run. In Run 17 the initially molded cross–section had a lateral slope of about 30 degrees. The bottom width was 11 cm, the top width was 23.5 cm, and the depth was about 6.1 cm. The initial depth of flow was somewhat less than that of the cross–section.

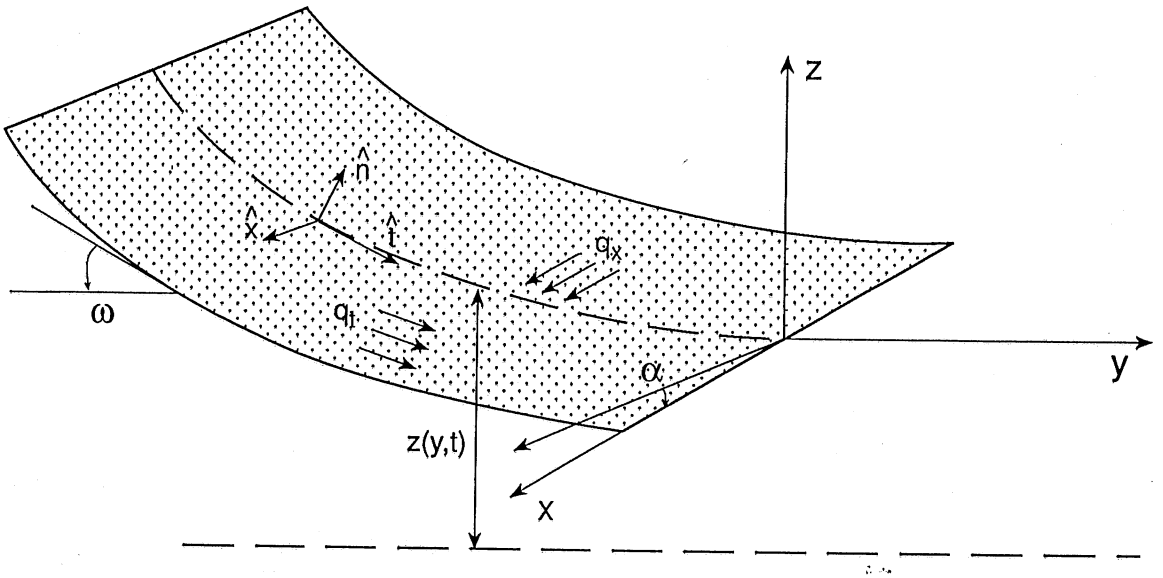

Figure 2.5. Two–dimensional bedload transport.

The experiment was continued for a total run time of 12 hours, after which a dynamically stable state had been attained. The water discharge was held at 4130 cm^3/s throughout the run. The streamwise slope of the channel was set to be 1/466, or 0.00215. The sediment was essentially uniform in size, with a median diameter of 1.3 mm.

For the numerical simulation, the same initial cross–sectional shape and input parameters were used. The calculation was continued so as to simulate the entire 12 hours of run time. The numerical program fixed the discharge at 3900 cm^3/s, a value close to that of the actual experiment.

In Figure 2.6, the results of the flow field modeling can be seen. These include the velocity distribution, the shear stress distribution and the discretization of the domain with triangular elements at time = 12 hours.

In Figure 2.2, the time evolution of the cross–section is illustrated. It is seen how the front of erosion migrates up the bank. It is also seen that the process slows down asymptotically, approaching the state of dynamic equilibrium.

In Figures 2.7 and 2.8, the experimental results for Run 17 of Ikeda (1981) are compared against the results of the calculation. Two different bedload models are used in the calculation. The notation K–P refers to the formulation of Kovacs and Parker (1991a) described above. The notation P–A refers to a previous formulation based on that presented in Parker and Andrews (1985). It can be seen that the present nonlinear, vectorial bedload calculation is a better tool for estimating the time evolution of water surface width (Figure 2.7) and the channel center depth (Figure 2.8). The rather lower depths realized in the experiment appear to be due to a notable decrease in roughness height during the run, something that cannot be predicted by the numerical model.

Figure 2.9 shows the streamwise bedload transport rate of the half cross–section as it approaches the final dynamic equilibrium value.

Figure 2.10 provides a good summary to this section. It provides a non–dimensional collapse of the time evolution of channel geometry of the cross–section. It is noteworthy that near the dynamic equilibrium state there is a portion of the bed near the axis of symmetry that is nearly flat. There is a smooth transition from the flat portion to the bank, making it possible to allow for streamwise sediment transport in the central portion of the channel without further erosion of the bank. In order to describe the evolution toward the cross–sectional geometry associated with this dynamic equilibrium, correct modeling of the shear stress distribution so as to reflect the transverse turbulent momentum transport is of vital importance.

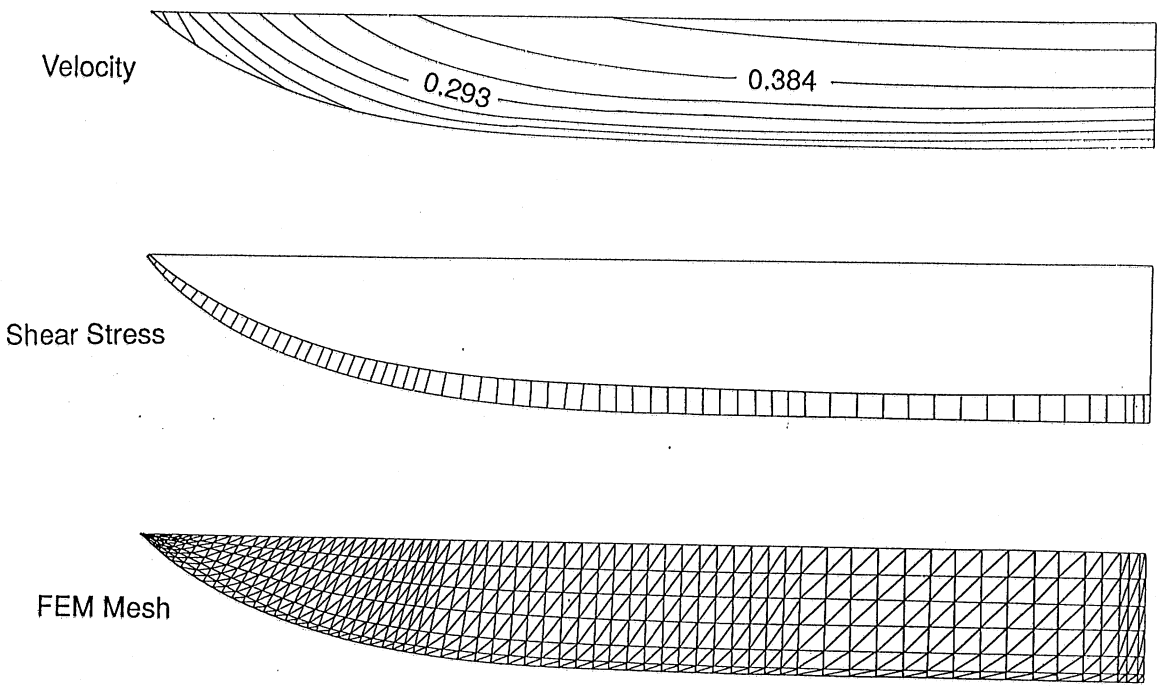

Figure 2.6. Results from the modeling of the flow field.

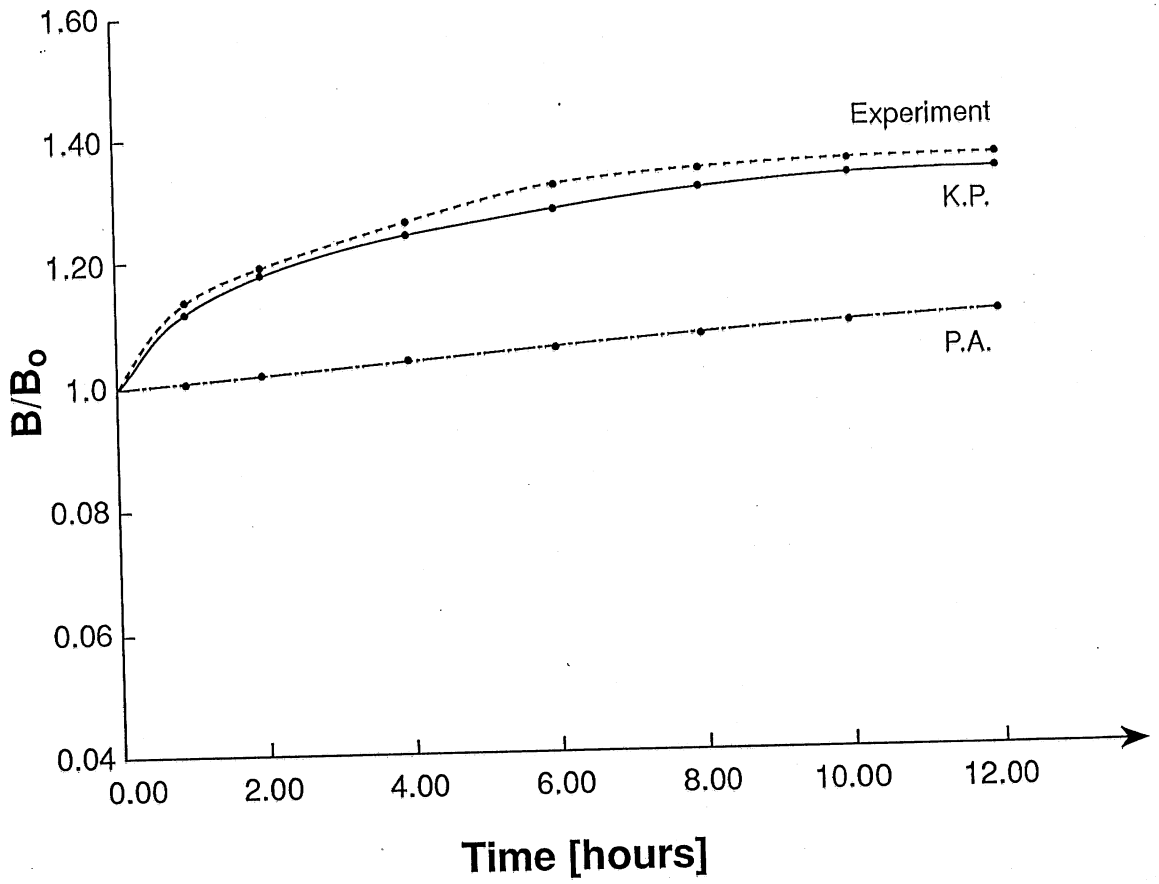

Figure 2.7. Comparison, water surface width.

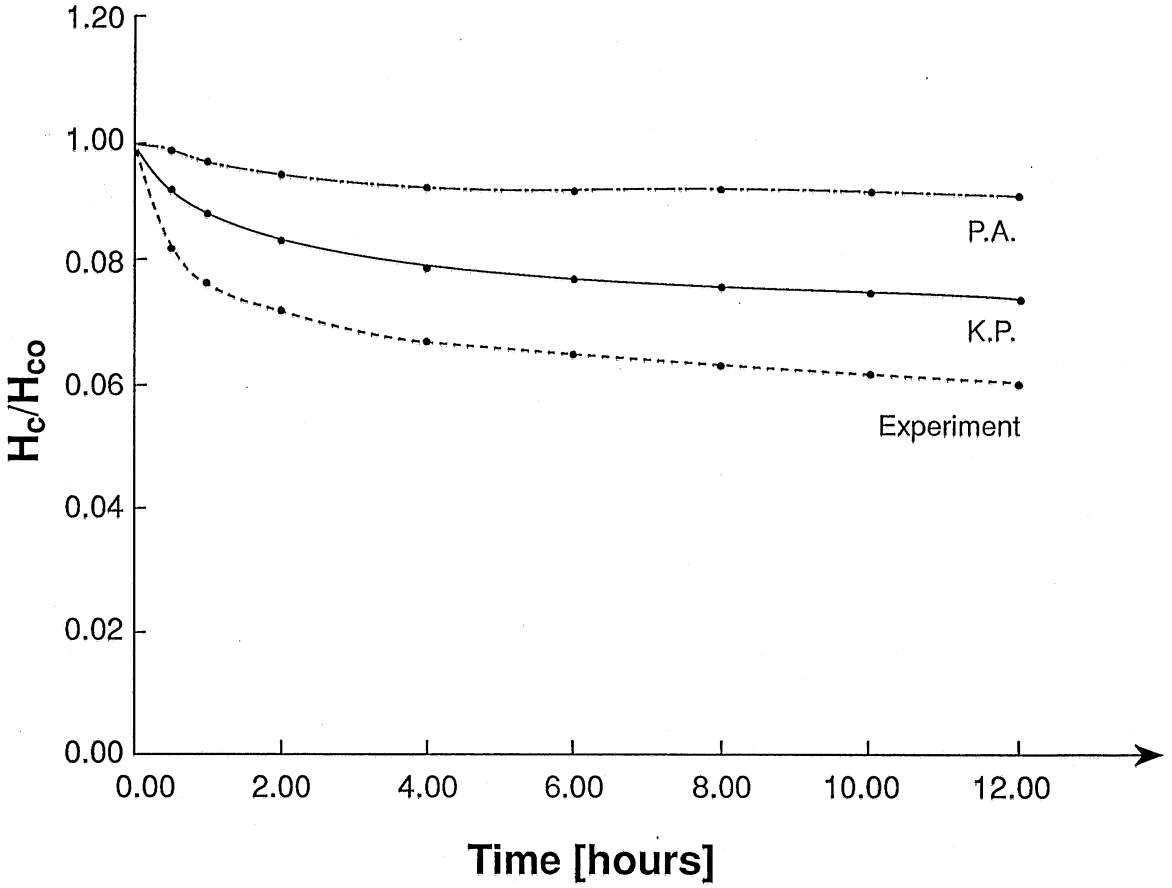

Figure 2.8. Comparison, depth in the center of the channel.

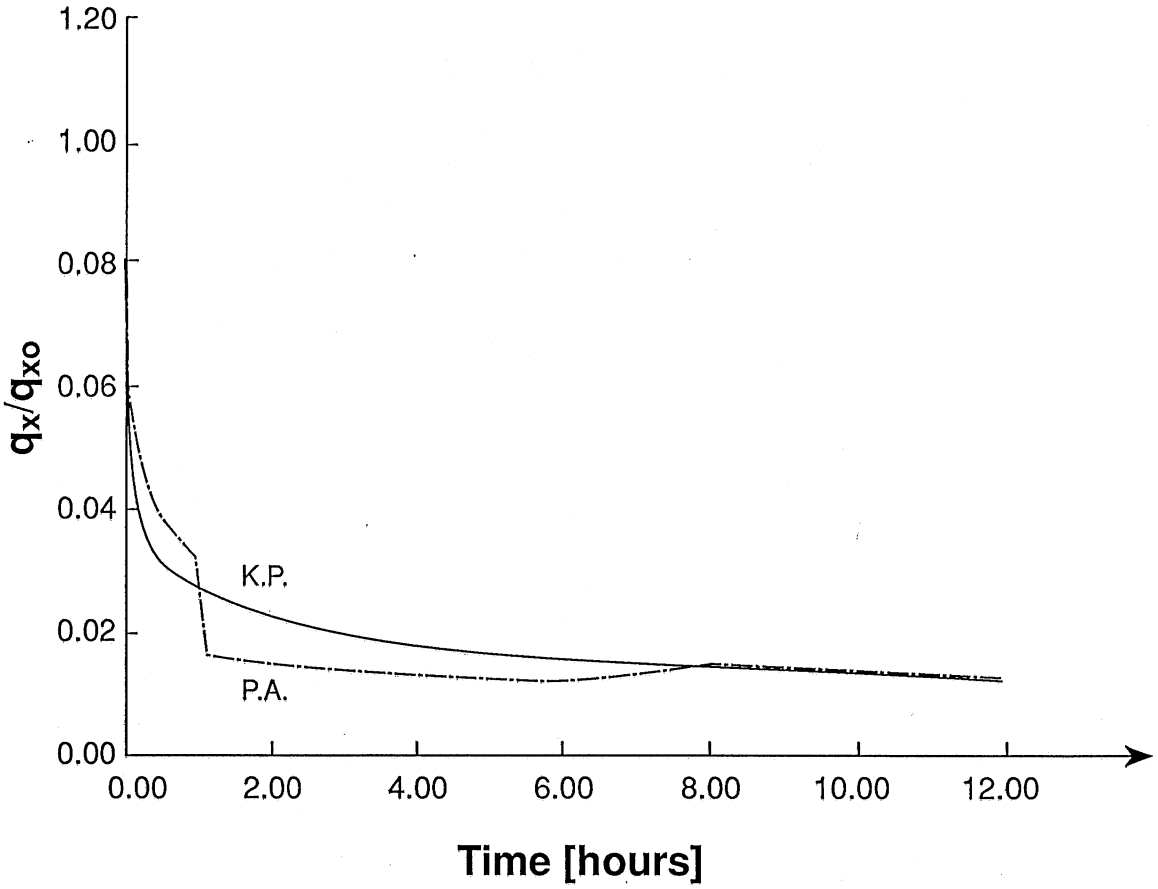

Figure 2.9. Streamwise bedload rate of the half cross–section.

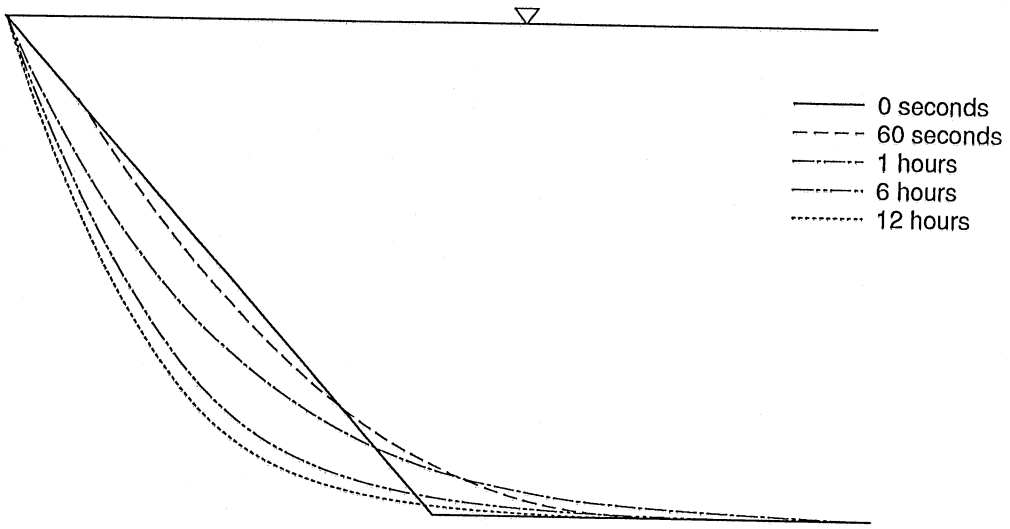

Figure 2.10. Non–dimensional channel geometry in time.

2.5 FURTHER RESEARCH

As mentioned in the introduction, the numerical model will be complete with the inclusion of the effect of distributed drag such as permeable dikes, as well as the transport of suspended sediment. Numerical modeling of permeable dikes implies that the governing differential equation of the flow field will have an extra term associated with distributed resistance. In the case of suspended sediment, another partial differential equation describing the conservation of suspended sediment has to be solved on the domain of the flow field.

Expansion of the present numerical model will be complete in the near future: the entire numerical project will constitute the body of the Ph.D thesis of the second author of this report, Agnes Kovacs.

2.6 CONCLUSION

The numerical model described here provides a tool for the detailed analysis of the time evolution of the cross–section of straight river channels. It will also be possible to model different methods of bank protection such as permeable dikes. Having gained a deeper understanding of the development of straight river channels, more complicated problems such as meandering, sorting etc. likely be investigated more successfully in the future.

2.7 REFERENCES

Bagnold, R. A. 1956 The flow of cohesionless grains in fluids. *Proc. Roy. Soc. London.* 249. No. 964.

Ikeda, I. 1981 Self–formed straight channels in non–cohesive bed materials. Part I. Experiments. *Report of Dept. of Found. Eng. & Const. Eng., Saitama Univ.* 10. 17–35.

Kovacs, A. & Parker, G. 1991a Time development of straight self–formed river channels in non–cohesive material. Part 1. General vectorial model for bedload transport on arbitrarily sloping beds. Ms. in preparation for submission to *Journal of Fluid Mechanics.*

Kovacs, A. & Parker, G. 1991b Time development of straight self–formed river channels in non–cohesive material. Part 2. Finite element modeling of time evolution of channel cross–sectional shape. Ms. in preparation for submission for *Journal of Fluid Mechanics.*

Parker, G. & Andrews, E. D. 1985 Sorting of bedload sediment by flow in meander bends. *Water Resources Research* 14. 127–144.